



1 **TITLE**

2 **Seismic survey in urban area: the activities of the EMERSITO INGV**  
3 **emergency group in Ancona (Italy) following the 2022 Mw 5.5 Costa**  
4 **Marchigiana-Pesarese earthquake**

5  
6 **Authors:** Daniela Famiani (1), Fabrizio Cara (1), Giuseppe Di Giulio (2), Giovanna Cultrera  
7 (1), Francesca Pacor (3), Sara Lovati (3), Gaetano Riccio (4), Maurizio Vassallo (2), Giulio  
8 Brunelli (3), Antonio Costanzo (11), Antonella Bobbio (5), Marta Pischiutta (8), Rodolfo  
9 Puglia (3), Marco Massa (3), Rocco Cogliano (4), Salomon Hailemichael (1), Alessia Mercuri  
10 (1), Giuliano Milana (1), Luca Minarelli (2), Alessandro Di Filippo (5), Lucia Nardone (5),  
11 Simone Marzorati (10), Chiara Ladina (10), Debora Pantaleo (10), Carlo Calamita (10), Maria  
12 Grazia Ciaccio (1), Antonio Fodarella (4), Stefania Pucillo (4), Giuliana Mele (1), Carla Bottari  
13 (6), Gaetano De Luca (7), Luigi Falco (4), Antonino Memmolo (4), Giulia Sgattoni (9),  
14 Gabriele Tarabusi (9)

15  
16 **Affiliation:**

- 17 (1) Istituto Nazionale di Geofisica e Vulcanologia, Sezione di Roma1, Roma, Italy.  
18 (2) Istituto Nazionale di Geofisica e Vulcanologia, Sezione di Roma1, L'Aquila, Italy.  
19 (3) Istituto Nazionale di Geofisica e Vulcanologia, Sezione di Milano, Milano, Italy.  
20 (4) Istituto Nazionale di Geofisica e Vulcanologia, Sezione Irpinia, Grottaminarda, Italy.  
21 (5) Istituto Nazionale di Geofisica e Vulcanologia, Sezione Osservatorio Vesuviano,  
22 Napoli, Italy.  
23 (6) Istituto Nazionale di Geofisica e Vulcanologia, Sezione Osservatorio Etneo, Catania,  
24 Italy.  
25 (7) Istituto Nazionale di Geofisica e Vulcanologia, Sezione Osservatorio Nazionale  
26 Terremoti, L'Aquila, Italy.  
27 (8) Istituto Nazionale di Geofisica e Vulcanologia, Sezione di Roma2, Roma, Italy.  
28 (9) Istituto Nazionale di Geofisica e Vulcanologia, Sezione di Bologna, Bologna, Italy.  
29 (10) Istituto Nazionale di Geofisica e Vulcanologia, Sezione Osservatorio Nazionale  
30 Terremoti, Ancona, Italy.  
31 (11) Istituto Nazionale di Geofisica e Vulcanologia, Sezione Osservatorio Nazionale  
32 Terremoti, Rende, Italy.

33  
34 **Correspondence to:**

35 Fabrizio Cara [fabrizio.cara@ingv.it](mailto:fabrizio.cara@ingv.it)  
36 Daniela Famiani [daniela.famiani@ingv.it](mailto:daniela.famiani@ingv.it)

37 **Abstract**

38 This paper illustrates the activities of EMERSITO, an emergency task force of the *Istituto*  
39 *Nazionale di Geofisica e Vulcanologia* (INGV, Italy) devoted to site effects and microzonation  
40 studies, during the seismic sequence that occurred close to the Adriatic coast in Central Italy  
41 since November 9th, 2022, following the Mw 5.5 mainshock localised in the sea. In particular,  
42 we describe the steps that led to the deployment of a temporary network of seismic stations in  
43 the urban area of Ancona, the main city of the Adriatic coastline. Data collected by the  
44 temporary Ancona network (identification code 6N, doi: [10.13127/sd/qctgd6c-3a](https://doi.org/10.13127/sd/qctgd6c-3a), EMERSITO  
45 Working Group, 2024) from November 2022 to the end of February 2023 have been



46 preliminary analysed with different techniques to characterise the deployment sites, and are  
47 now available for further and detailed studies.

## 48 1. Introduction

49 On November 9th, 2022, at 06:07:24 UTC (07:07:24 local time), a  $M_w$  5.5 earthquake localised  
50 in the Adriatic Sea struck the Marchigiana-Pesarese coast in Central Italy (Fig. 1). Due to its  
51 magnitude, exceeding the threshold of 5.0, and the closeness to urban areas (Fano and Pesaro  
52 are about 30-35 km, Ancona 45 km far from the epicenter), *Istituto Nazionale di Geofisica e*  
53 *Vulcanologia* (National Institute of Geophysics and Volcanology, INGV<sup>1</sup>) soon activated the  
54 Seismic Crisis Unit to monitor the ongoing seismic sequence. Among several tasks, the Crisis  
55 Unit coordinates the INGV emergency task forces<sup>2</sup> devoted to specific issues and scientific  
56 support for the activities of the Civil Protection: SISMICO<sup>3</sup> (Moretti et al. 2023), for adding  
57 seismic stations in the epicentral area to improve the localization of the seismic events of the  
58 sequence, EMERGEO<sup>4</sup> for investigating the surface geological effects, QUEST<sup>5</sup> for the  
59 macroseismic survey and EMERSITO<sup>6</sup> for site effects and seismic microzonation studies. In  
60 general, the INGV task forces<sup>2</sup> operate synergistically although with a different intervention  
61 timing. In particular, SISMICO<sup>3</sup>, EMERGEO<sup>4</sup> and QUEST<sup>5</sup> start their activities within a few  
62 hours to 1-2 days after the mainshock. EMERSITO<sup>6</sup> activities, on the contrary, usually start  
63 from 2 to 7 days after the main seismic event, depending on the level of damage caused by the  
64 mainshock and, therefore, the accessibility to the epicentral area where the site effect are often  
65 more evident (Cara et al. 2019).

66  
67 In this paper, we focus on the activities of EMERSITO<sup>6</sup> working group following the  $M_w$  5.5  
68 mainshock in the Adriatic sea. The area of the Adriatic coast where the earthquake was felt was  
69 very broad, approximately ranging from the cities of Rimini and Ancona that are about 90 km  
70 far from each other (Fig. 1). However, the level of damage, reported by both the fire brigade  
71 and the QUEST<sup>5</sup> surveys, was very low (maximum IV MCS), so the logistics left us some  
72 options to plan an intervention for site effects studies. After several considerations,  
73 EMERSITO<sup>6</sup> decided to deploy a temporary seismic network in the urban area of Ancona, the  
74 regional capital of Marche. This choice was driven by: a) the relative high values of peak  
75 ground acceleration (PGA) recorded for the mainshock (the maximum PGA has been recorded  
76 in Ancona at IV.PCRO station with  $197 \text{ cm/s}^2$  on the EW component); b) the damage and  
77 evacuations reported by the fire brigade and the technicians of Marche region; c) the strong  
78 lithological heterogeneities in town; d) the scientific interest in improving the approach for the  
79 evaluation of the local seismic response in urban areas.

80  
81 The deployment of the network started 4 days after the mainshock and was completed in three  
82 days, also taking advantage of the presence of an INGV office in Ancona<sup>7</sup> and with the  
83 collaboration of the municipality and of the Marche Region technicians. During the emergency,  
84 which lasted from November 2022 to March 2023, EMERSITO<sup>6</sup> carried out four public reports  
85 to describe its activities (Cara et al., 2022a, 2022b, 2022c; Famiani et al., 2023).

86  
87 In this paper we describe in detail the EMERSITO<sup>6</sup> network, the data collected and some  
88 preliminary analyses.

## 89 90 2. Deployment of the temporary network

### 91 92 2.1 Seismological and geological framework



93 The 2022 Mw 5.5 seismic sequence struck the Adriatic coast and affected some major towns,  
94 such as Pesaro, Rimini, Fano, Senigallia and Ancona among others (Fig. 1). This latter city  
95 (about 100.000 citizens) is the administrative center of the Marche region and one of the main  
96 seaports of the Adriatic Sea. Before this event, in the previous century Ancona was hit by  
97 significant earthquakes: in 1930 (epicenter close to Senigallia city, 10-15 km far from Ancona,  
98 estimated Mw 5.8 and MCS intensity VIII; Guidoboni et al. 2018, Rovida et al. 2020 and 2022;  
99 see Fig. 1) and more recently in 1972 by an important seismic sequence (Kissilinger 1972,  
100 Console et al. 1973) that lasted 11 months. The shocks of the 1972 sequence were short in  
101 duration but showed rather high values of PGA; the strongest earthquake occurred on June 14,  
102 with magnitude Mw 4.7 and estimated MCS intensity VIII. The epicenter of this event was  
103 localized in the Adriatic sea in front of the Ancona seaport (Fig. 1), at about 10 km from Ancona  
104 downtown in the NE direction (Rovida et al, 2017). The city experienced diffuse but moderate  
105 damage with 7000 of 35000 buildings declared unusable. More than 30.000 people left their  
106 homes. At the end of the 1972 sequence, Ancona was the object of the first large-scale seismic  
107 monitoring in Italy, with the deployment of a network (Ferraris et al., 1975) followed by an  
108 extensive microzonation survey of the area (Calza et al., 1981). The reconstruction, also in  
109 downtown, was exemplary for the Italian standards and followed strict anti-seismic rules.  
110 During the 2022 mainshock, localized at a distance of about 45 km from Ancona (see Fig. 1),  
111 the city experienced some negligible damage and evacuations, as reported by the regional  
112 technicians and the Fire Brigade (Fig. 2). As for the 1972 event, higher levels of PGA were  
113 recorded during the main shock compared with instrumented sites at similar distance  
114 (Engineering Strong Motion Database-ESM<sup>8</sup>, Luzi et al., 2020). A subset of the recorded PGA  
115 values are reported in Table 1 (see also Figure 1 for details in the position of the considered  
116 instrumented sites).

117  
118  
119  
120  
121

**Table 1:** PGA recorded by some stations of the two permanent networks in Italy, IV (<https://doi.org/10.13127/SD/X0FXnH7QfY>) and IT (<https://doi.org/10.7914/SN/IT>), ordered by epicentral distance. The two stations in Ancona are highlighted in bold.

<i>Network</i>	<i>Station</i>	<i>Locality</i>	<i>Epicentral distance (km)</i>	<i>Horizontal PGA (cm/s<sup>2</sup>)</i>
IV	COR1	Corinaldo	49.3	31.610
<b>IT</b>	<b>ANB</b>	<b>Ancona</b>	<b>48.8</b>	<b>166.424</b>
IV	FCOR	Fonte Corniale	48.6	21.796
<b>IV</b>	<b>PCRO</b>	<b>Ancona</b>	<b>47.9</b>	<b>197.842</b>
IT	CTL	Cattolica	47.3	31.749
IV	CRTC	Cartoceto	44.2	22.409
IV	SENI	Senigallia	34.6	139.209
IV	FANO	Fano	30.5	52.613

122  
123  
124  
125  
126  
127

From a geological point of view, Ancona is characterized by strong lithological heterogeneity and represents a scientifically interesting case for the evaluation of the local seismic response in an urban area. Moreover, the western area of Ancona is built on a deep landslide (Stucchi et al., 2005; Stucchi and Mazzotti, 2009). In 1982, after a period of heavy rain, the landslide moved suddenly (Crescenti et al., 2005), involving several suburban districts of Ancona:



128 Posatora, Borghetto and partially Torrette (Fig. 3). The movement of the landslide damaged  
129 two hospitals and the Faculty of Medicine of the University, 280 buildings were destroyed and  
130 overall 865 homes damaged, the railway was torn up and the coastal road was damaged along  
131 a front of approximately 2.5 kilometers. The disaster forced the authorities to evacuate 3,661  
132 people from the affected area. Nowadays the landslide zone, as well the aquifer, is constantly  
133 monitored through an early-warning system (Cardellini and Osimani, 2013) and it is still in  
134 very slow movement (Agostini et al., 2014).

135

136 The Ancona area falls in the marginal part of the central Apennines thrust system, where Mio-  
137 Plio-Pleistocene terrigenous deposits overlie a mostly carbonate succession referable to the  
138 Umbria-Marche succession (Cello and Tondi, 2013). In the periadriatic sector, the geological  
139 structures related to the origin of the central Apennine chain are generally buried under the  
140 foredeep turbidite successions that sedimented starting from the Miocene age (Bally et al.,  
141 1986). In particular, in the area of Ancona (Fig. 4), this foredeep succession is mainly  
142 characterized, in its upper part, by Pleistocene gray-blue marly clays (*Argille Azzurre*, FAA  
143 formation). During the Late Pliocene there was an intense phase of regional uplift that in the  
144 Middle Pleistocene, resulted in the emergence of the external part of the Marche region from  
145 the sea level. Subsequently, and in relation to the different climatic phases, there were erosion  
146 processes of various intensity (also stasis), and sedimentation. All these phenomena modeled  
147 the landscape defining the current morphostructural arrangement of the region and producing  
148 alluvial, eluvial-colluvial marine and landscape deposits widely outcropping in the study area.  
149 The recent anthropization and urbanization are strongly altering the original morphology, in  
150 particular in the coastal area, introducing erosion and accumulation processes that are  
151 considerably more rapid and intense than those due to natural causes (Farabollini et al. 2000).  
152 The outcropping marine succession in Ancona has been classified into four lithostratigraphic  
153 units from bottom to top:

- 154 a) *Schlier* formation (SCH)
- 155 b) Chalky-sulfur formation (GES)
- 156 c) *Colombacci* formation (FCO)
- 157 d) *Argille azzurre* formation (FAA)

158 SCH formation (Late Miocene age, hemipelagic origin) diffusely outcrops along the coastline  
159 and consists of quite stiff marls and calcareous marls, with expected thickness up to 250 mt.

160 GES unit (Late Miocene, evaporitic origin) consists of bituminous clays, sulfiferous limestones  
161 and whitish nodular chalk banks. Also this formation outcrops along the coastline and has a  
162 maximum thickness of 40-50m.

163 The *Colombacci* formation (FCO, late Miocene age) is mainly composed of clays and marly-  
164 silty clays. The maximum thicknesses are greater than 100 m.

165 FAA formation (early Pliocene-early Pleistocene) widely outcrops in Ancona area (thickness  
166 up to 300 m) and it is a pelitic succession that in its upper part consists of massive gray-blue  
167 stratified marly clays with rare sand lenses. It is worth noting that this unit has strong lateral  
168 and vertical variations.

169

170 The quaternary deposits in Ancona, according to the 282 sheet of the 1 : 50.000 Geological  
171 Map of Italy (Lettieri, 2009), have been merged into the *Musone River* syntheme: the eluvial-  
172 colluvial deposits (MUS<sub>b2</sub>) cover sometimes large sectors of the hillsides, the surfaces of the  
173 terraces, and fill the bottom of most of the valleys. Thickness can be up to 10-15m and they  
174 consist of fine sediments (sands, clays and silts).

175 Quaternary slope instabilities (Agostini et al., 2014) affect areas at east and west of Ancona,  
176 characterized by Plio-Pleistocene clay soils (e.g., Centamore et al., 1982; Cancelli et al., 2005;  
177 Fiorillo 2003). The landslide deposits, whenever it was possible to represent them on a 1:25000



178 map, have been distinguished as unstable (MUSa1) or stable (MUSa1q). The Ancona landslide,  
179 at west of Ancona, represents one of these instabilities.

180  
181 The alluvial deposits (MUSbn) comprise the terraces and consist of heterometric silt-gravel  
182 units. They are spread over the city of Ancona and their thickness is variable from point to  
183 point but of the order of 15-50 m. In the more urbanized areas they can be completely covered  
184 by anthropic sediments, 2m thick, consisting of coarse calcareous pebbles mixed to the old  
185 natural soil.

186

## 187 **2.2 EMERSITO INGV intervention**

188 EMERSITO<sup>6</sup> is the INGV task force devoted to site effect and microzonation studies during  
189 significant seismic crises in Italy. As for other INGV task forces<sup>2</sup>, EMERSITO<sup>6</sup> is activated for  
190 earthquakes exceeding magnitude 5.0 or whenever the observed damage is likely due to local  
191 amplification effects. Since its official constitution in 2015, the group consists of a variable  
192 number of people, to date about 50 INGV employees on a voluntary basis, among researchers,  
193 technicians and technical collaborators, and involves various INGV departments and offices  
194 spread in the Italian territory. An operational protocol regulates the operation of the group,  
195 organised by two national coordinators that lead a management team that includes a contact  
196 person for each INGV office. EMERSITO<sup>6</sup> worked in the 2016-2017 Central Italy seismic  
197 sequence (Cara et al., 2019; Priolo et al. 2020; Milana et al., 2020) and the 2017 Ischia  
198 emergency (Nardone et al., 2023), but the group participated, in an unofficial form, also to  
199 previous Italian emergencies (San Giuliano di Puglia 2002, Palermo 2002, L'Aquila 2009,  
200 Emilia-Romagna 2012), increasing its experience in this research field.

201

202 From the beginning of the emergency, EMERSITO<sup>6</sup> started its activities by organizing itself in  
203 specific working groups mainly to collect a variety of information regarding the epicentral area:  
204 geology, damage surveys, previous studies on site effects and microzonation, seismic data by  
205 nearby stations of the National Seismic Network run by INGV (Rete Sismica Nazionale-RSN;  
206 INGV Seismological Data Centre, 2006) and the Italian Strong Motion Network run by the  
207 Civil Protection (Rete Accelerometrica Nazionale-RAN, PCM-CPD, 1972). This information  
208 has been uploaded in an online Web-GIS project (Fig. 5), shared and updatable in real time by  
209 all the users located in different offices of INGV. This procedure was useful for sharing the  
210 knowledge of the area and the ideas on the intervention through live and virtual meetings,  
211 which guided the preliminary field inspections and the deployment of the seismic temporary  
212 network.

213

214 The initial planning was carried out remotely considering the available Level 1 Seismic  
215 Microzonation study, that incorporates noise measurements, downholes and boreholes with  
216 stratigraphy (<https://qmap-protciv.regione.marche.it/cs/>) and the preliminary evidence of  
217 earthquake-induced damage coming from the other INGV Task Forces (SISMIKO<sup>3</sup>,  
218 EMERGE<sup>4</sup> and QUEST<sup>5</sup>). QUEST<sup>5</sup> in particular has provided first indications about the most  
219 damaged areas in terms of affected buildings (Tertulliani et al., 2022): they reported a  
220 macroseismic intensity of V EMS-98 for Ancona and individuated state of damage up to degree  
221 3 in some buildings in downtown and damage 1-2 degree in a suburban neighbourhood for  
222 some recent reinforced concrete buildings (vulnerability class C and D). Afterwards, the Fire  
223 Brigade performed a detailed survey for all buildings, distinguishing the levels of damage in  
224 the city (Fig. 2).

225 Ad hoc site inspections were carried out in collaboration with the INGV Ancona<sup>7</sup> office, which  
226 has become a logistic support for all the task forces. It was then possible to contact several  
227 institutions, i.e. the Marche Region (Albarello et al., 2022), the Regional Civil Protection, the



228 Municipality of Ancona and the Navy Headquarter in Ancona. They were really collaborative,  
229 giving us suitable places for the station deployments, helping in finding further investigations  
230 and technical reports in the vicinity of the sites. The final choice of the sites was also made on  
231 the basis of fast single-station ambient noise measurements, in order to have a first-order  
232 evaluation of possible resonance effects.

233 As aforementioned, the city suffered a low level of damage, then it did not have any major  
234 impact on its usual activities. For this reason, installations inside buildings have been preferred  
235 to guarantee continuous power supply and security of the seismic stations. We then identified  
236 ground floors, basements or courtyards of private and public buildings, such as schools,  
237 universities, sports centers, the Palace of the Regione Marche and religious structures.

238 Although EMERSITO<sup>6</sup> intervention was not focused on the landslide hazard, we decided to  
239 install one station (CMA10) in the western part of Ancona, where the deep landslide moved in  
240 1982.

241  
242 After this preliminary phase, the final configuration of the temporary EMERSITO<sup>6</sup> network  
243 covered the urban area of Ancona municipality and consisted of 11 six-channels digitizers,  
244 coupled to velocimetric (Lennartz 3D-5 sec) and accelerometric (Kinometrics Episensor)  
245 sensors. Fig. 4 illustrates the position of the seismic stations in relation with the outcropping  
246 geology, while Table 2 shows their location, coordinates, date of installation and data  
247 transmission mode. The EMERSITO<sup>6</sup> temporary seismic network was registered in  
248 the Federation of Digital Seismograph Networks (FDSN<sup>9</sup>) with the network code 6N<sup>10</sup>. At the same  
249 time, station codes have been registered with the International Seismological Center (ISC<sup>11</sup>).  
250 Most of the stations are installed close to the most damaged areas (compare with Fig. 2),  
251 CMA06 is in the new industrial area in the south, CMA10 in the 1982 landslide area, close to  
252 the district of Posatora.

253  
254 A difficult task was the identification of sites characterized by the presence of outcropping stiff  
255 lithologies where to install a reference station. After several tests, we found a possible reference  
256 site on the so-called Colombacci formation (FCO), i.e. clay-marls of Miocene age, at about 90  
257 mt from IV.PCRO station, free from clear resonance effects on noise, and installed the  
258 reference station CMA15 (Fig.s 4 and 6).

259 The topography at Ancona downtown is not flat (Fig. 6). The medium elevation is about 70mt  
260 but there are some hills that reach about 180-250 m and quickly slope towards the Adriatic sea.  
261 Stations CMA15 and IV.PCRO are on a hill 140-160 m high whereas station CMA12 was  
262 placed on the top of a hill 100 m high that quickly slopes towards the Adriatic sea and where  
263 there is also the lighthouse of Ancona (Fig. 6). To avoid possible soil-interaction with the  
264 lighthouse, the station was placed at about 30mt from it, inside a building of the Navy facilities.

265  
266  
267  
268  
269

**Table 2.** List of the sites of the 6N seismic network. The dismissing date of the stations was 24th of February 2023.

<i>Name</i>	<i>Location</i>	<i>Lat</i>	<i>Lon</i>	<i>Installation date</i>	<i>Acquisition mode</i>
CMA05	Piaget School	43.618437	13.52708	2022-11-15 10:40	Real Time
CMA06	Paolinelli Sports Center, in the hamlet of Baraccola	43.553738	13.511387	2022-11-15 11:32	Real Time
CMA07	Salesian Oratory	43.605702	13.503745	2022-11-13 18:03	Real Time
CMA08	Economics University	43.620228	13.516387	2022-11-14 15:12	Real Time



CMA09	Church of Saints Cosma and Damiano	43.618237	13.515918	2022-11-13 11:12	Real Time
CMA10	Via della Grotta (landslide)	43.603008	13.480115	2022-11-14 11:18	Real Time
CMA11	Navy	43.598542	13.506017	2022-11-14 16:05	Stand Alone
CMA12	Cardeto park (lighthouse)	43.622585	13.51589	2022-11-15 10:40	Stand Alone
CMA13	Via Barilatti	43.593848	13.502273	2022-11-15 13:33	Stand Alone
CMA14	Raffaello Palace	43.609948	13.509390	2022-11-15 16:07	Stand Alone
CMA15	Palascherma	43.608372	13.531515	2022-11-15 16:08	Stand Alone

270

271 Figure 7 shows the 1D stratigraphic models under the installation sites, based on the available  
272 boreholes close to the stations and to our interpretation about the geological evolution of the  
273 area. The information used for the construction of these 1D stratigraphic models were located  
274 at a distance between 5 and 250 meters from the stations, determining different levels of  
275 reliability and uncertainty in the models, especially for the non-outcropping layers, considering  
276 the lateral variability and the different thickness and lithologies encountered.

277 The models reach a depth of 100 meters and are characterized by a variable thickness of  
278 altered/fractured layers. In particular, CMA06-CMA07-CMA11 stations, installed in flat valley  
279 areas, are composed of fine alluvial unconsolidated deposits (MUSb2) above the clayey  
280 formation of Argille Azzurre (FAA). CMA05-CMA08-CMA09-CMA13-CMA14-CMA15  
281 stations are installed in quite flat areas and their stratigraphy featured by fine and more  
282 heterometric colluvial unconsolidated deposits (MUSb2, MUSbn) above the clayey (Argille  
283 Azzurre FAA) or marly (Schlier, SCH) or clayey/marly (Argille a Colombacci, FCO)  
284 geological formations. CMA10 is installed on the 1982 landslide sediments (MUSa1) whereas  
285 CMA12 is set on SCH formation in a topographic relief.

286

### 287 3. Seismic data collection of the 6N network

#### 288 3.1 Data availability

289 The installation of the seismic stations was completed in three days and the 6N network was  
290 fully operative for 3 months, from November 13th, 2022, until February 24th, 2023.

291 The six stations in real-time acquisition mode (Table 2) transmitted data as well as their state  
292 of health (SOH), such as input voltage and quality of GPS signal received, to the EMERSITO<sup>6</sup>  
293 servers. Data availability and SOH were frequently checked with dedicated software tools.  
294 During the acquisition period, several maintenance interventions were carried out to download  
295 data from stand-alone stations and to verify their correct operation.

296 Raw data were converted into the standard binary *miniSEED* format, and organized in a  
297 structured seismic archive (following the SeisComP data structure). Then, data quality and  
298 completeness were checked, and all the relevant information was used for creating the metadata  
299 volumes with the perspective to upload them in the INGV node of the European Integrated  
300 Data Archive portal (EIDA<sup>13</sup>; Danecek et al., 2021).

301 All continuous data have been transferred to EIDA<sup>13</sup> and are currently available to everyone  
302 interested in. The dataset acquired by the EMERSITO<sup>6</sup> temporary network 6N<sup>10</sup> and described  
303 in this manuscript can be accessed under [10.13127/sd/qctgd6c-3a](https://doi.org/10.13127/sd/qctgd6c-3a) (EMERSITO Working  
304 Group, 2024), according to a set of rules defined by the INGV data management office (Open  
305 Data Portal-ODP<sup>12</sup>) and EMERSITO<sup>6</sup>.

306

307 Figure 8 shows availability of recordings for each station of the 6N network as a function of  
308 time. The gaps in the records of some stations were caused by some malfunctions, in general



309 due to power failures; however, data completeness turned out to be quite satisfactory for all the  
310 stations, being on average about 97%.

311

### 312 **3.2 Data quality**

313 In order to characterize the seismic background noise at the seismic stations of the temporary  
314 EMERSITO<sup>6</sup> 6N<sup>10</sup> network, we computed the Power Spectral Density (PSD) using the three-  
315 component continuous signals.

316 PSD and Probability Density Functions (PDF) were obtained from the waveform data and the  
317 corresponding response files using the PPSD<sup>14</sup> class of ObsPy<sup>15</sup>, a Python toolbox for  
318 Seismology (Beyreuther et al., 2010), in which the computation of PSD and PDF is based on  
319 the algorithm proposed by McNamara and Buland (2004). For each seismic channel, the  
320 software computes the PDF from the distribution of the PSD values at each spectral interval,  
321 providing the probability of occurrence of a given seismic signal level in a fixed frequency  
322 interval.

323 We used the 90th percentile curves to get a robust estimate of the noise level and to compare it  
324 between different stations, as shown in Figure 9 for the three components of motion. They are  
325 often above the reference curves (new high and new low noise models, NHNM and NLNM  
326 respectively) as computed by Peterson (1993). This was expected because the stations are  
327 located in a highly urbanized area. The high noise level occurs mainly at frequencies above 1  
328 Hz during day times, and there is a strong reduction of the noise level during night times (about  
329 10-15 dB) and also during day times on Christmas holidays (by about 5 dB) (Fig. S1a in  
330 Supplementary material).

331

332 The inspection of spectral and time amplitude levels allowed us to evaluate the suitability of  
333 the installation sites and find critical situations. In particular, the CMA10 station was initially  
334 installed inside a shelter that hosts electronic devices for monitoring movements of the active  
335 landslide. This situation negatively affected the data quality of this station (Fig. S1b in  
336 Supplementary material) with evident disturbances on the recordings. Consequently, the station  
337 was moved outside the structure, about 2 meters away from the previous position, obtaining an  
338 improvement in the data quality, with more stable and lower amplitude spectra (although some  
339 artefacts are still present at about 20 sec).

340

### 341 **3.3 Recorded earthquakes**

342 During the operating time of network 6N<sup>10</sup> there were 258 aftershocks of the Marchigiana-  
343 Pesarese seismic sequence with  $2.0 \leq M \leq 2.9$ , 28 with  $3.0 \leq M \leq 4.0$  and 1 with  $M = 4.2$ , that  
344 was the strongest one after the mainshock (Fig. 10a). Eight  $M \geq 3.0$  events are related to other  
345 local seismic sources in Italy located at a maximum distance of 100km from Ancona (Fig. 10b).  
346 Of course not all the local events have been recorded by the stations of network 6N or, although  
347 recorded, not all of them have a good quality.

348 Seven  $M \geq 4.0$  events have an epicentral distance ranging from 100 to 500 km (Fig. 10c) and  
349 the network was also able to record the strong Turkish earthquake that occurred the 6th of  
350 February 2022 (Mwpd 7.9) at a distance of about 2200 km from Ancona (Fig. 10d).

351

352 Figure 11 shows an example of the  $M_w$  3.9 aftershock of December 8<sup>th</sup> at 07:08 UTC recorded  
353 by some 6N<sup>10</sup> stations. The seismograms and the spectrograms highlight clear differences in  
354 the site response: CMA12 and CMA15 sites, located on stiff units (FCO and SCH formations,  
355 respectively), are characterized by short durations and small amplitudes, whereas stations  
356 installed on poor sediments over stiffer materials (CMA10, CMA13 and CMA14) show longer  
357 durations and higher amplitudes. The spectrograms also point out frequency variations.





358 Some differences can be also observed for low-frequency events, such as the teleseismic Mw<sub>pd</sub>  
359 7.9 Turkish earthquake(Fig. 12).

360  
361

#### 362 4. Preliminary analyses

363 The recordings of ambient vibrations and earthquakes collected by the 6N<sup>10</sup> network allowed  
364 us to perform some preliminary analyses for characterising the recording sites. Moreover, the  
365 joint use of data of the temporary networks installed during the emergency, as the 6N one, and  
366 of the permanent networks, in principle increase the chance to improve the estimates of the  
367 earthquakes' parameters (i.e. their localization and focal mechanism).

368 We first present the different techniques used for the analyses and some illustrative results. The  
369 overall results for each station of the network are presented as synthetic sheets collected in the  
370 supplementary material.

371

##### 372 4.1 Localization and Focal mechanism improvements

373 The availability of the local events recorded by network 6N<sup>10</sup>, as well of other networks,  
374 increase the chance to get better localization and to constrain the calculations of the focal  
375 mechanisms, especially for the earthquakes where the first polarities can be depicted.

376 As an example, we used data of two events (see Table 3) recorded simultaneously by 3  
377 networks: 6N<sup>10</sup>, Y1 (managed by SISMICO INGV emergency task force; D'Alema et al., 2022,  
378 Moretti et al., 2023) and IV (RSN; INGV Seismological Data Centre, 2006). For event  
379 #33466171 using only data from IV and Y1 it was not possible to calculate the focal  
380 mechanism. Therefore we added the 6N data; first, using the phase picks from the seismograms,  
381 we relocated the event by using a multi-parameter procedure (Ciaccio et al., 2021) that explores  
382 the hypocenter solutions space by changing the *a-priori* key conditions that strongly influence  
383 the solution convergence in the linearized approach. Then, we computed the double-couple  
384 fault plane solutions from P-wave first motion data (FPFIT program, Reasenber and  
385 Oppenheimer, 1985). Finally, because our data allowed a significant increase of the sampling  
386 of the focal sphere, the procedure successfully calculated the focal mechanism of the event  
387 (Fig. 13). This focal mechanism shows a transpressive solution, is of good quality in terms of  
388 uncertainties on strike, dip, rake (quality code QP= A) and station distribution ratio (STDR  
389 <0.5), being this last quantity sensitive to the distribution of the data on the focal sphere  
390 (Reasenber and Oppenheimer, 1985).

391 The same procedure was followed for the event #33589291 (Table 3). In this case, the focal  
392 solution was already available, but adding 6N data improved the STRD quantity (from 0.6 to  
393 0.55) giving greater robustness to the solution.

394

395 **Table 3.** Location and focal mechanism parameters of the two analyzed seismic events. EventID: numerical  
396 unique identifier of the INGV earthquakes database (<http://terremoti.ingv.it>).

397

EventID	Date	Magnitude	Latitude	Longitude	Depth (km)	Strike	Dip	Rake
33466171	2022-11-23T01:59:26	M <sub>L</sub> 3.6	43.9337	13.2537	15.75	100	50	30
33589291	2022-12-08T05:30:04	M <sub>w</sub> 3.6	43.8975	13.2653	15.14	110	40	30

398

399

#### 400 4.2 Data analysis methods



401 **4.2.1 Horizontal-to-Vertical spectral ratio on noise (HVNSR) and earthquakes**  
 402 **(HVSr)**

403 The Horizontal-to-Vertical spectral ratio on noise (HVNSR) and earthquakes (HVSr) data play  
 404 an important role in seismic microzonation and site effects studies (Hailemichael et al., 2020).  
 405 Indeed they are widely used and can provide information on the resonance frequencies of the  
 406 site, which is related to the thicknesses of the layers and their average shear wave velocity.

407  
 408 The HVNSR analysis (Nakamura, 1989), although not able to define the transfer function of  
 409 the site, can provide useful indications on the possible resonance frequencies and on the  
 410 susceptibility of a site towards possible amplification phenomena. To estimate the HVNSR at  
 411 the Ancona network, we used the HVNEA software on the continuous recordings (Vassallo et  
 412 al., 2023) which takes advantage of the Geopsy software (Wathelet et al., 2020). The  
 413 computation results in hourly HVNSR curves as average on 120s windows and repeated over  
 414 the entire duration of the acquisition (about 3 months). At the end, we produced 1.600 to 2.200  
 415 hourly HVNSR curves for each station.

416  
 417 The HVSr analysis is conceptually similar to HVNSR, but is performed on earthquakes rather  
 418 than on noise. Similarly to HVNSR, HVSr was performed with the software HVNEA,  
 419 described in Vassallo et al. (2023). For each event, HVSr is calculated on a 6-second window  
 420 from the theoretical S-wave arrival time. The averages were obtained by using a subset of  
 421 events from the INGV earthquake bulletin<sup>16</sup>, using a circular search of magnitude  $M \geq 3$  events  
 422 at a maximum distance of 50 km from Ancona city (Table 4). With these criteria, the considered  
 423 earthquakes had a signal-to-noise ratio (SNR)  $\geq 3$  in the frequency range 0.5-15.0 Hz. The  
 424 number of selected events ranges from 17 to 29, then the results are indicative.

425  
 426  
 427

**Table 4.** List of the earthquakes used for HVSr and SSR analysis

#EventID	Time	Latitude (degrees)	Longitude (degrees)	Depth (Km)	Author	MagType	Magnitude	EventLocationName
33378441	2022-11-14T23:10:54.960000	43.9368	13.3483	5.2	BULLETIN-INGV	$M_L$	3.5	Costa Marchigiana Anconetana (Ancona)
33389921	2022-11-16T08:57:08.040000	43.934	13.337	4.4	SURVEY-INGV	$M_L$	3.2	Costa Marchigiana Anconetana (Ancona)
33418361	2022-11-19T03:56:03.320000	43.9767	13.3195	10.8	SURVEY-INGV	$M_L$	3.0	Costa Marchigiana Pesarese (Pesaro-Urbino)
33431491	2022-11-20T05:20:30.250000	43.9027	13.2642	10.3	SURVEY-INGV	$M_W$	4.2	Costa Marchigiana Pesarese (Pesaro-Urbino)
33431631	2022-11-20T05:23:19.770000	43.9677	13.3185	8.7	SURVEY-INGV	$M_L$	3.2	Costa Marchigiana Pesarese (Pesaro-Urbino)
33434911	2022-11-20T09:59:46.700000	43.9083	13.3353	9.2	SURVEY-INGV	$M_L$	3.3	Costa Marchigiana Anconetana (Ancona)
33435461	2022-11-20T10:38:54.300000	43.9625	13.2825	7.9	SURVEY-INGV	$M_L$	3.3	Costa Marchigiana Pesarese (Pesaro-Urbino)
33466171	2022-11-23T01:59:26.800000	43.91	13.2288	10.2	BULLETIN-INGV	$M_L$	3.6	Costa Marchigiana Pesarese (Pesaro-Urbino)



33477031	2022-11-24T17:26:40.160000	43.925	13.2753	9.1	SURVEY-INGV	M <sub>L</sub>	3.2	Costa Marchigiana Pesarese (Pesaro-Urbino)
33477901	2022-11-24T22:11:30.200000	43.904	13.2937	9.5	SURVEY-INGV	M <sub>L</sub>	3.2	Costa Marchigiana Pesarese (Pesaro-Urbino)
33533041	2022-12-01T00:03:02.130000	43.8888	13.3305	9.7	SURVEY-INGV	M <sub>L</sub>	3.4	Costa Marchigiana Anconetana (Ancona)
33534141	2022-12-01T04:42:07.310000	43.8875	13.339	8.8	SURVEY-INGV	M <sub>L</sub>	3.2	Costa Marchigiana Anconetana (Ancona)
33584401	2022-12-07T11:06:10.980000	43.9202	13.3133	10.0	SURVEY-INGV	M <sub>L</sub>	3.0	Costa Marchigiana Pesarese (Pesaro-Urbino)
33589291	2022-12-08T05:30:05.540000	43.913	13.297	9.1	BULLETIN-INGV	M <sub>w</sub>	3.6	Costa Marchigiana Pesarese (Pesaro-Urbino)
33590351	2022-12-08T06:55:41.970000	43.954	13.3127	9.1	SURVEY-INGV	M <sub>L</sub>	3.0	Costa Marchigiana Pesarese (Pesaro-Urbino)
33590571	2022-12-08T07:08:18.650000	43.914	13.2888	8.4	BULLETIN-INGV	M <sub>w</sub>	3.9	Costa Marchigiana Pesarese (Pesaro-Urbino)
33591681	2022-12-08T08:06:50.860000	43.9312	13.3175	8.9	SURVEY-INGV	M <sub>L</sub>	3.3	Costa Marchigiana Pesarese (Pesaro-Urbino)
33645871	2022-12-14T08:34:05.690000	44.0173	13.2392	9.1	SURVEY-INGV	M <sub>L</sub>	3.0	Costa Marchigiana Pesarese (Pesaro-Urbino)
33683471	2022-12-19T07:37:13.480000	43.8762	13.3748	8.8	SURVEY-INGV	M <sub>L</sub>	3.3	Costa Marchigiana Anconetana (Ancona)
33771681	2022-12-31T00:37:35.720000	43.9827	13.3077	8.8	SURVEY-INGV	M <sub>L</sub>	3.1	Costa Marchigiana Pesarese (Pesaro-Urbino)
33804101	2023-01-04T15:55:18.660000	43.939	13.275	9.5	BULLETIN-INGV	M <sub>L</sub>	3.5	Costa Marchigiana Pesarese (Pesaro-Urbino)
33804361	2023-01-04T16:01:18.420000	43.9262	13.2773	8.7	SURVEY-INGV	M <sub>L</sub>	3.3	Costa Marchigiana Pesarese (Pesaro-Urbino)
33870151	2023-01-12T07:06:14.500000	43.9117	13.2668	9.6	BULLETIN-INGV	M <sub>L</sub>	3.6	Costa Marchigiana Pesarese (Pesaro-Urbino)
33959201	2023-01-21T18:52:37.040000	43.9348	13.3682	7.7	SURVEY-INGV	M <sub>L</sub>	3.2	Costa Marchigiana Anconetana (Ancona)
33977501	2023-01-25T14:30:20.590000	43.9682	13.3052	7.9	SURVEY-INGV	M <sub>L</sub>	3.0	Costa Marchigiana Pesarese (Pesaro-Urbino)
34020401	2023-02-02T04:18:22.520000	43.9823	13.3227	7.0	SURVEY-INGV	M <sub>L</sub>	3.2	Costa Marchigiana Pesarese (Pesaro-Urbino)



34024531	2023-02-02T14:49:37.610000	43.9583	13.2907	7.2	SURVEY-INGV	M <sub>L</sub>	3.1	Costa Marchigiana Pesarese (Pesaro-Urbino)
34161341	2023-02-21T00:07:20.490000	43.2798	13.3392	7.4	BULLETIN-INGV	M <sub>w</sub>	3.6	1 km NW Pollenza (MC)

428

429

430

#### 4.2.2 Directional amplification in frequency and time domain

431 Directional amplification effects imply that there is a preferential direction of amplification of  
432 the horizontal Fourier spectra, reported as a strike from the geographic north, as firstly proposed  
433 by Bonamassa and Vidale (1991). In the time domain, they correspond to linearly polarized  
434 ground motion, with mean polarization along the direction of maximum amplification.

435 In this work, directional amplification effects are preliminarily investigated in the frequency  
436 domain through the calculation of rotated horizontal-to-vertical spectral ratios both on noise  
437 (HVNSR) and earthquakes (HVSr), and in the time domain by using the covariance matrix  
438 analysis (Kanasewich, 1980; Jurkevics 1988).

439 The use of rotated spectral ratios was first introduced by Spudich et al. (1996) and subsequently  
440 exploited by several authors to detect the horizontal polarization of ground motion on  
441 topography and in fault zones (e.g., Rigano et al., 2008; Di Giulio et al., 2009; Pischiutta et al.,  
442 2012) or on sedimentary basins (Theodoulidis et al., 2018).

443 For the computation on noise, we used the Geopsy software (Whatelet et al., 2020) applying  
444 an anti-trigger algorithm to select the most stationary part of the signals, as well as a cosine  
445 taper and a Konno-Ohmachi smoothing filter with coefficient  $b = 40$  (Konno and Ohmachi,  
446 1998). We calculated HVNSR after rotating the NS and EW components by steps of  $10^\circ$ , from  
447  $0^\circ$  to  $180^\circ$ .

448 For earthquakes we considered the same list in Table 4 used for HVSr analysis. We first cut a  
449 portion of each event, a 6-seconds long window, including the S and early coda waves. Then,  
450 we computed the direction of maximum amplification as the azimuth at which the HVSr peak  
451 reaches the maximum value. Conventionally, the directional amplification effect is considered  
452 significant if the ratio between the maximum and minimum amplitude levels at the frequency  
453 peak exceeds 1.5 (Pischiutta et al., 2018). The complete values retrieved by the rotated HVNSR  
454 and HVSr are given in the Supplementary material (Tables S1 and S2, corresponding to results  
455 from earthquake and ambient noise recordings, respectively).

456

457 The covariance matrix method in the time domain (Jurkevics, 1988) is an alternative method  
458 to estimate the ground motion polarization both on noise and earthquakes, in particular when  
459 directional peaks have been observed with the rotated HVNSR or HVSr. The method results  
460 in the estimation of the polarization ellipsoid. In order to give a quantitative evaluation on how  
461 much elongated the polarization ellipsoids is, we apply the hierarchical criterion proposed by  
462 Pischiutta et al. (2012), which results are given in the supplementary material (Tables S1 and  
463 S2, corresponding to results from earthquake signals and ambient noise, respectively).

464

#### 4.2.3 Horizontal-to-Horizontal spectral ratio (SSR)

466 The Horizontal-to-Horizontal spectral ratios (SSR) technique is based on the assumption that  
467 the ratio between horizontal Fourier spectra from earthquakes recorded at a given site and at a  
468 bedrock site represent a good estimate of the transfer function of the site. The implicit  
469 assumption is that the contribution of the source and the crustal propagation is the same for the  
470 two sites, and that the spectrum of the rock site (i.e. the reference station) is free from  
471 amplification effects (Borcherdt, 1970; Cara et al., 2011). For these reasons, this technique is



472 believed to give the seismic response of a given site, not only limited to the resonance effects  
473 as for HVNSR or HVSR.

474 For network 6N<sup>10</sup> we chose CMA15 station as the most suitable reference site, being installed  
475 on an outcropping geological bedrock (FCO, Colombacci Formation). Moreover, its recordings  
476 are characterized by short duration, small amplitudes and no resonance frequency peaks (see  
477 Figures 11 and 14).

478 In order to automate the calculation, a script implemented in a Python environment and based  
479 on the ObsPy<sup>15</sup> framework (Beyreuther et al., 2010) was used. The code allows to: (1) extract  
480 the signal related to a seismic event over a time window of definable duration (6s in this case)  
481 starting from the arrival of the S wave, which has been estimated using the technique proposed  
482 by Akazawa (2004); (2) calculate the signal-to-noise ratio (SNR); (3) process the signals with  
483 a Konno and Ohmachi (1998) filter and, finally, calculate the SSR ratios. The iterative  
484 application was applied on the same list of HVSR analysis taking into account the simultaneous  
485 presence of events on both the considered site and the reference site (Table 4).

486

#### 487 **4.3 Summary results**

488 This subsection illustrates the results of the techniques described in the previous sections, by  
489 using three selected stations as representative of the network: CMA08, CMA14 and CMA15.  
490 The results for all the stations of the 6N network are given as synthetic sheets and collected in  
491 the supplementary material (Figures from S3 to S13).

492

493 Figure 14 shows the HVNSR, HVSR and SSR results for the three considered stations. In the  
494 following we summarize some preliminary conclusions:

495

- 496 a) HVNSR amplitudes are relatively low (about 2 in average) and no clear resonance  
497 peaks are observed.
- 498 b) HVNSR and HVSR of station CMA15 are flat, as expected for a reference site.
- 499 c) HVSR curves of CMA08 and CMA14 are slightly different from HVNSR ones: the  
500 amplitudes are higher and also the frequency peaks depicted by the two techniques are  
501 different. It should be considered that the number of earthquakes used for HVSR is not  
502 very high, therefore the result is only indicative.
- 503 d) SSR analysis shows very different outcomes than HVSR analysis. This behavior could  
504 be due to the choice of the reference site (CMA15), and/or to possible 2- or 3-  
505 dimensional site effects not accounted for by the HVSR technique.

506

507 The analysis of HVNSR carried out over the entire recording period was also important to  
508 assess the temporal stability of the spectral peaks at each site (see Fig. S2 in Supplementary  
509 material). There was no relevant variation of the peak frequencies whereas the peak amplitude  
510 shows temporal variations up to 20%. These variations are mostly related to day-night spectral  
511 levels reduction, especially in the vertical components and above 4 Hz.

512

513 Results of directional and polarization analyses, on both earthquake and noise, are shown in  
514 Figure 15 for two stations, CMA08 and CMA14.

515 For station CMA08 the rotated HVNSR and HVSR highlights the presence of a directional  
516 peak at about 3-4 Hz, and along N90°-110° azimuth (roughly, E-W direction). The pattern is  
517 more complex at station CMA14 (Fig. 15, bottom panels), where earthquakes and noise give  
518 slightly different outcomes. Earthquake recordings show two clear peaks in the HVSR analysis,  
519 the former at 2.6 Hz, with maximum amplification roughly N-S and the latter at 4.4 Hz that is  
520 not directional. Circular histograms of polarization azimuths obtained from filtered earthquake  
521 signals in the frequency band 1-3 Hz, show a similar trend in N-S direction.



522

523 **6. Data Availability**

524 Data described in this manuscript can be accessed under 10.13127/sd/qctgd6c-3a (EMERSITO  
 525 Working Group, 2024).

526

527 **7. Discussion and conclusions**

528 The aims of this work were to illustrate the seismic dataset collected by the 6N temporary  
 529 network at Ancona, stored and available from the EIDA database, describe the intervention of  
 530 the EMERSITO working group and focus on the difficulties that can be encountered in urban  
 531 contexts during emergency activities, and finally to present the preliminary results that can be  
 532 achieved during a seismic sequence.

533

534 The overall results of HVSR and polarization analysis on both earthquakes and noise are  
 535 summarized in Figure 16.

536 As aforementioned, the HV on noise does not detect some frequency peaks, which are evident  
 537 only by earthquake data (CMA05, CMA06, CMA09, and CMA14), and, for some other peaks,  
 538 displays lower amplitude and/or no directionality (CMA05, CMA07, CMA09, CMA12,  
 539 CMA14). HVNSR and HVSR for station CMA10, which is set on the 1982 landslide, have a  
 540 shape with no clear resonance peak.

541

542 In terms of directional motion the results between noise and earthquakes are fully consistent  
 543 only at stations CMA08, CMA11, and CMA15.

544

545 Table 5 lists, for each 6N<sup>10</sup> station, the outcropping lithology, the number of peaks observed  
 546 on HVSRs and for each one, the peak frequency and amplitude values. When amplification is  
 547 found to be directional, the direction of maximum amplification and polarization is given as  
 548 well.

549 The lowest resonance frequency value from data analysis (Table 5), observed at the sites  
 550 CMA07, CMA11 and CMA15, is around 1.5 Hz (frequency range 1-2.5 Hz in Fig. 16) and  
 551 related to thick clay deposits (Fig. 7). The majority of sites show  $f_0$  values in the range 2.5-5  
 552 Hz. Higher frequencies ( $f_0 > 5$  Hz) are observed at two stations (CMA12 and CMA05) closest  
 553 to the sea in the northern direction, where the Schlier marly Formation is nearly outcropping  
 554 (Fig. 7).

555

556 **Table 5.** Synthesis of results of directional analysis (frequency and amplitude values of resonance peaks) obtained  
 557 from HVSR and HVNSR analysis.

558

Summary of HVSR and HVNSR analyses							
Station	Site conditions	N. peaks	#	Frequency peak (Hz)	Ampl.	Direction max ampl. (degrees)	Notes
CMA05	SCH - Schlier Fm.	2	1	5.2□5.6	2.7□4.1	30□36	HVSRs indicate no directionality
	Marly limestones and clays (Miocene)		2	9.7	2.8□3.6	12□20	Peak evident only on HVSRs

560



	<b>CMA06</b>	<b>MUSbn - Musone Fm.</b>	2	1	1.2□1.3	2.4□2.9	none	
561		Terrace deposits (Holocene)		2	3.5□3.7	2.7□4.7	none	Peak evident only on HVSRs
	<b>CMA07</b>	<b>MUSbn - Musone Fm.</b>	1	1	1.6□2.2	2.1□3.5	30□60	HVNSRs have lower amplitudes than HVSRs
562		Terrace deposits (Holocene)						
	<b>CMA08</b>	<b>Musb2- Musone Fm.</b>	1	1	2.8□3.9	2.3□3.5	80□110	
563		Eluvio-colluvial deposits (Holocene)						
	<b>CMA09</b>	<b>Musb2 Musone Fm.</b>	2	1	1.7□2.4	2.1□3.3	170	HVNSRs have lower amplitudes than HVSRs and no directionality
564		Eluvio-colluvial deposits (Holocene)		2	3.5□3.7	2.7□4.7	80	Peak evident only on HVSRs
	<b>CMA10</b>	<b>Musa1 - Musone Fm.</b>	3	1	2.6□2.7	2.1	none	Peak evident only on HVSRs
		Active landslide deposits		2	4.1□4.4	2.3	0	Peak evident only on HVSRs
565		(Holocene)		3	5.3□7.5	2□3.2	none	Broadband peak
	<b>CMA11</b>	<b>MUSbn - Musone Fm.</b>	1	1	1.4□1.5	2.1□3.3	none	
566		Terrace deposits (Holocene)						
	<b>CMA12</b>	<b>SCH - Schlier Fm.</b>	1	1	8.8□9.6	2.5□3.7	100	HVSRs indicate no directionality
567		Marly limestones and clays (Miocene)						
	<b>CMA13</b>	<b>MUSbn - Musone Fm.</b>	1	1	1.4□2.6	2□3.6	10	HVNSRs have lower amplitudes than HVSRs and no directionality
568		Terrace deposits (Holocene)						
	<b>CMA14</b>	<b>FAA - Argille Azzurre Fm.</b>	2	1	2.2□2.6	2□2.7	140□170	HVNSRs have lower amplitudes than HVSRs
569		Marly and silty clays (Pleistocene)		2	4.4□4.5	2.5□3.2	none	Peak evident only on HVSRs
	<b>CMA15</b>	<b>FCO - Colombacci Fm.</b>	no peaks					
570		Marly clays with conglomeratic levels (Miocene)						

570  
 571

572 However, it is important to say that for a complete geological-based interpretation, the  
 573 earthquake database collected during the experiment needs to be fully analyzed, with a detailed  
 574 search of  $M < 3.0$  events with  $SNR \geq 3$ , to have more robust statistics.

575

576 At the stage of the activities of EMERSITO during the seismic sequence, we can infer some  
 577 points to be investigated in detail in future papers:



- 578 a) The HVNSR technique was a good method to test the functioning of the stations and  
579 the variability in an urban context, but it seems that for this case study, where the  
580 geological features do not show strong impedance contrast, is not very suitable for  
581 revealing resonance effects.
- 582 b) Also the HVSR technique, even if it has to be refined with a greater number of  
583 earthquakes, shows similar trends of HVNSR but with higher amplitudes and more  
584 evident peaks.
- 585 c) The SSRs are strongly different from HVNSR and HVSR. Also SSR has to be refined  
586 with a greater number of earthquakes, but the role of the reference station needs to be  
587 investigated. If the SSRs will result reliably, the next step will be to compare these  
588 amplification estimates with numerical simulations based on the available geological  
589 profiles for each site. Therefore, the use of 1D, 2D and maybe 3D simulations hopefully  
590 will explain the observed amplification pattern.
- 591 d) Although the role of landslide sediments in the amplification pattern is out of the aim  
592 of this work, we believe that specific and multidisciplinary studies based on extensive  
593 measurements in the unstable zones of the city are needed. It has to be taken into  
594 account that in unfavorable hydrological conditions, seismic waves of a possible  
595 moderate-to-strong earthquake could trigger the landslide movements.
- 596 e) All the stations (except CMA06 and CMA14 situated in external courtyards) are  
597 installed in the basement floors into buildings, then the interaction between soil and  
598 structures can have played a role in the observed results.





599        **Acknowledgements.** We thank the people of Ancona who hosted the instruments. In  
600        particular we thank the Navy and the Regione Marche for all the support, facilities and  
601        information that they have made available.  
602        We gratefully acknowledge the Laboratory ESITO of INGV  
603        ([https://www.ingv.it/monitoraggio-e-infrastrutture/laboratori/laboratorio-effetti-di-](https://www.ingv.it/monitoraggio-e-infrastrutture/laboratori/laboratorio-effetti-di-sito)  
604        sito) for the technical support during the experiment.  
605        We also thank the Italian Department of Civil Defence (DPC) for the economic support  
606        and a special thanks to the INGV group, in particular Massimo Fares, Diego Franceschi  
607        and Ivano Carluccio that helped us in the procedure to share the data of the network 6N  
608        in EIDA and Mario Locati for the INGV data policy task.

609  
610

#### 611        **Details on dataset access.**

612        **The best way for downloading data from EIDA is to use the Orfeus Data**  
613        **Center WebDC3 Web Interface**

614  
615

**Repository:** <http://www.orfeus-eu.org/webdc3/>

616        Go to the “Explore Stations” tab, set Network Type as “All temporary nets” and  
617        Network Code as “6N\*+ (2022) - Emersito Seismic Network in Ancona (Central  
618        Italy)”. Select the HN (velocimetric data) or EH (accelerometric data) channels or both.  
619        Then press “Search”. A list of the available seismic stations appears, it is possible to  
620        select all or only the desired stations.

621        Go to the “Submit request” tab and set the appropriate Time Selection Window. If you  
622        wish to download the complete records, set the time windows from 9-11-2022 to 28-  
623        02-2023 which include the whole recording period of the network 6N. Unfortunately  
624        the Orfeus Data Center limits the maximum size of data that can be downloaded for  
625        each request at about 1.5Gb. This means that it is possible to download up to 30 days  
626        of the HN (velocimetric) channels or up to 15 days of the EH (accelerometric) channels  
627        of one station at a time. Anyhow, to reduce the waiting times we suggest halving the  
628        request, e.g. 15 days for station and HN channels.

629        You can also choose to request for the miniseed data only, the metadata in XML format  
630        or the metadata in text format.

631        If everything is ok go to the “Download Data” tab, where you can follow the status of  
632        the FDSNWS requests. At the end click on the “SAVE” button to download the  
633        requested data.

634        **Author's contribution:** F. Cara, G. Di Giulio, M. Vassallo, G. Cultrera, G. Riccio, S.  
635        Lovati and F. Pacor are the coordinators of the Emersito task force. They designed and  
636        managed the experiment, so they contributed to the project administration and the  
637        conceptualization tasks. D. Famiani has been charged as scientific manager for the  
638        experiment, supervised by the coordinators. She wrote the initial draft of this  
639        manuscript that was revised and completed by the coordinators, in particular by F. Cara,  
640        G. Cultrera, G. Di Giulio and F. Pacor.



641 G. Di Giulio, M. Vassallo, D. Famiani, G. Brunelli, A. Bobbio, M. Pischiutta, S.  
642 Hailemikael, A. Mercuri, G. Milana, L. Minarelli, A. Di Filippo, L. Nardone, S.  
643 Marzorati, C. Ladina, D. Pantaleo, and C. Calamita contributed to the investigation,  
644 finding the sites, deploying the seismic stations and maintaining them.  
645 M. Vassallo, G. Riccio, A. Costanzo, A. Bobbio, M. Pischiutta, M. Massa, R. Puglia,  
646 S. Hailemikael, A. Mercuri, G. Milana, M.G. Ciaccio, S. Pucillo, G. Sgattoni and C.  
647 Ladina contributed to the formal analysis.  
648 G. Riccio was in charge of data curation.  
649 G. Brunelli contributed to the definition of 1D stratigraphy models under the  
650 investigated sites.  
651 R. Cogliano contributed to the maintenance of the web-gis whereas S. Pucillo, A.  
652 Fodarella, G. Brunelli and D. Famiani helped in finding resources to add to the web-  
653 gis.  
654 G. Mele and C. Bottari helped the coordinators in the initial dissemination of the  
655 experiment, useful also for the writing of this manuscript.  
656 L. Falco G. and A. Memmolo contributed to the instrumental part, in particular in the  
657 setting of the real-time stations.  
658 M. Massa, G. Mele and C. Bottari, G. De Luca, G. Sgattoni and G. Tarabusi contributed  
659 to the initial ideas about the experiment and also to the resources.

660 **Competing interests:** The authors declare that they have no conflict of interest.



661

### Footnotes

662

<sup>1</sup> <https://www.ingv.it/en/index.php>

663

<sup>2</sup> <https://www.ingv.it/en/monitoring-and-infrastructure/emergencies/emergency-groups>

664

<sup>3</sup> <https://sismiko.ingv.it/>

665

<sup>4</sup> <https://emergeo.ingv.it>

666

<sup>5</sup> <https://quest.ingv.it>

667

<sup>6</sup> <http://emersitoweb.rm.ingv.it/index.php/it/>

668

<sup>7</sup> <http://www.an.ingv.it/>

669

<sup>8</sup> [https://esm-db.eu/#/event/INT-20221109\\_0000046](https://esm-db.eu/#/event/INT-20221109_0000046)

670

<sup>9</sup> <https://www.fdsn.org/>

671

<sup>10</sup> [https://fdsn.org/networks/detail/6N\\_2022/](https://fdsn.org/networks/detail/6N_2022/)

672

<sup>11</sup> <http://www.isc.ac.uk>

673

<sup>12</sup> <https://data.ingv.it/en/>

674

<sup>13</sup> <https://eida.ingv.it/en/>

675

<sup>14</sup> [https://docs.obspy.org/packages/autogen/obspy.signal.spectral\\_estimation.PPSD.html](https://docs.obspy.org/packages/autogen/obspy.signal.spectral_estimation.PPSD.html)

676

<sup>15</sup> <https://docs.obspy.org/>

677

<sup>16</sup> <http://terremoti.ingv.it/en/>

678

679

680



681

## References

- 682 Agostini, A., Tofani, V., Nolesini, T., Gigli, G., Tanteri, L., Rosi, A., Cardellini, S., and Casagli,  
683 N.: A new appraisal of the Ancona landslide based on geotechnical investigations and stability  
684 modelling, Quarterly Journal of Engineering Geology and Hydrogeology,  
685 <https://doi.org/10.1144/qjegh2013-028>, 2014.
- 686  
687 Akazawa, T.: A technique for automatic detection of onset time of P-and S-phases in strong  
688 motion records, 13th World Conference on Earthquake Engineering, Vancouver, Canada, Aug. 1–  
689 6. [https://www.iitk.ac.in/nicee/wcee/article/13\\_786.pdf](https://www.iitk.ac.in/nicee/wcee/article/13_786.pdf) [Accessed on 8 Dec 2023], 2004.
- 690  
691 Albarello, D., Pacitti, P., Schiaroli, A., Tiberi, P., Fantozzi, P. L., Pieruccini, P., and Madiati, C.:  
692 La microzonazione sismica delle Marche. 10 anni di attività, Regione Marche. ISBN 978-88-  
693 95554-40-2, <https://hdl.handle.net/2158/1325073>, 2022.
- 694  
695 Bally, A. W., Burbi, L., Cooper, C., and Ghelardoni, R.: Balanced sections and seismic reflection  
696 profiles across the central Apennines, Mem. Soc. Geol. It., 35, 257-310, 1986.
- 697  
698 Beyreuther, M., Barsch, R., Krischer, L., Megies, T., Behr, Y., and Wassermann, J.: ObsPy: A  
699 Python Toolbox for Seismology, Seismological Research Letters, 81(3): 530–533,  
700 <https://doi.org/10.1785/gssrl.81.3.530>, 2010
- 701  
702 Bonamassa, O., and Vidale, J. E.: Directional site resonances observed from aftershocks of the 18  
703 October 1989 Loma Prieta earthquake sequence, Bull. Seismol. Soc. Am., 81, 1945–1958,  
704 <https://doi.org/10.1785/BSSA0810051945>, 1991.
- 705  
706 Borchardt R. D.: Effects of local geology on ground motion near San Francisco Bay, Bulletin of  
707 the Seismological Society of America, 60(1): 29–61, <https://doi.org/10.1785/BSSA0600010029>,  
708 1970
- 709  
710 Calza, W., Maistrello, M., Marcellini, A., Morganti, C., Rampoldi, R., Rossi, B., Stucchi M., and  
711 Zonno, G.: Elementi di microzonazione dell'area anconetana, Pubbl. Prog. Final. Geodin., 430, 68  
712 pp., 1981.
- 713  
714 Cancelli, A., Marabini, F., Pellegrini, M. and Tonnetti, G.: Incidenze delle frane sull'evoluzione  
715 della costa adriatica da Pesaro a Vasto, Memorie della Società Geologica Italiana, 27, 555–568,  
716 1984
- 717  
718 Cara, F., Di Giulio, G., Cavinato, G.P. et al.: Seismic characterization and monitoring of Fucino  
719 Basin (Central Italy), Bull Earthquake Eng, 9, 1961–1985, <https://doi.org/10.1007/s10518-011-9282-2>, 2011.
- 720  
721  
722 Cara, F., Cultrera, G., Riccio, G. et al.: Temporary dense seismic network during the 2016 Central  
723 Italy seismic emergency for microzonation studies, Sci Data, 6, 182,  
724 <https://doi.org/10.1038/s41597-019-0188-1>, 2019.
- 725  
726 Cara, F., Di Giulio, G., Bagh, S. et al.: Gruppo Operativo EMERSITO-Evento sismico Costa  
727 Marchigiana 2022, Rapporto N. 1 del 09/11/2022, <http://hdl.handle.net/2122/15783>, in Italian,  
728 2022a.
- 729



- 730 Cara, F., Di Giulio, G., Cultrera, G., Pacor, F., et al.: Gruppo Operativo EMERSITO-Evento  
731 sismico Costa Marchigiana 2022, Rapporto N. 2 del 13/11/2022, <http://hdl.handle.net/2122/15785>,  
732 *in Italian*, 2022b.  
733
- 734 Cara, F., Di Giulio, G., Cultrera, G., Pacor, et al.: RAPPORTO N. 3 ATTIVITÀ DEL GRUPPO  
735 OPERATIVO EMERSITO A SEGUITO DELL'EVENTO SISMICO Costa Marchigiana Pesarese  
736 Mw 5.5 del 9/11/2022, <http://hdl.handle.net/2122/15795>, *in Italian*, 2022c.  
737
- 738 Cardellini, S., and Osimani, P. (2013). The Ancona Early Warning Centre, Instrumentation and  
739 Continuous Monitoring of the Landslides. In *Landslide Science and Practice* (Vol. 2, pp. 57–65).  
740 Springer Berlin Heidelberg. [https://doi.org/10.1007/978-3-642-31445-2\\_7](https://doi.org/10.1007/978-3-642-31445-2_7)  
741
- 742 Cello, G., and Tondi, E.: Note illustrative della Carta Geologica d'Italia alla scala 1: 50.000,  
743 Foglio 282 Ancona, Ancona, Servizio Geologico d'Italia-ISPRA e Regione Marche, pagg. 101, *in*  
744 *Italian, SELCA Firenze*, 2013.  
745
- 746 Centamore, E., Coltorti, M. et al.: Aspetti neotettonici e geomorfologici del Foglio 133–134  
747 (Ascoli Piceno–Giulianova). CNR-Progetto Finalizzato 'Geodinamica': Contributi conclusivi per  
748 la realizzazione della Carta Neotettonica d'Italia, 2, 371–386, 1982.  
749
- 750 Ciaccio, M. G., Di Stefano, R., Improta, L., Mariucci, M. T., and BSI Working Group: First-  
751 Motion Focal Mechanism Solutions for 2015–2019  $M \geq 4.0$  Italian Earthquakes, *Frontiers in Earth*  
752 *Science*, 9, 630116, <https://doi.org/10.3389/feart.2021.630116>, 2021.  
753
- 754 Console, R., Peronaci, F., and Sonaglia, A.: Relazione sui fenomeni sismici dell'Anconetano  
755 (1972), *Ann. Geofis., Suppl. al vol. XXVI*, 3-148, <https://doi.org/10.4401/ag-5033>, *in Italian*,  
756 1973.  
757
- 758 Crescenti, U., Calista, M., Mangifesta, M. and Sciarra, N.: The Ancona landslide of December  
759 1982, *Giornale di Geologia Applicata*, 1, 53–62, [https://doi.org/10.1474/GGA.2005-01.0-](https://doi.org/10.1474/GGA.2005-01.0-06.0006)  
760 [06.0006](https://doi.org/10.1474/GGA.2005-01.0-06.0006), 2005.  
761
- 762 D'Alema, E., Alparone, S., Augliera, P., Biagini, D., Calamita, C., Castagnozzi, A., Cavaliere, A.,  
763 Costanzo, A., Della Bina, E., Farroni, S., Galluzzo, D., Gasparini, A., Ladina, C., Lauciani, V.,  
764 Mandiello, A. G., Margheriti, L., Marzorati, S., Moretti, M., Pantaleo, D., ... Zuccarello, L.:  
765 Seismic Data acquired by the SISMIKO Emergency Group - Northern Marche Coast - Italy 2022 -  
766 T17 [Data set]. Istituto Nazionale di Geofisica e Vulcanologia (INGV),  
767 <https://doi.org/10.13127/SD/TBLKBA-3U6>, 2022.  
768
- 769 Danecek, P., Pintore, S., Mazza, S., Mandiello, A., Fares, M., and Carluccio, I.: The Italian node  
770 of the European integrated data archive, *Seismol. Res. Lett.*, 92(3), 1726–1737,  
771 <https://doi.org/10.1785/0220200409>, 2021.  
772
- 773 Di Giulio, G., Cara, F., Rovelli, A., Lombardo, G., and Rigano, R.: Evidences for strong  
774 directional resonances in intensely deformed zones of the Pernicana fault, Mount Etna, Italy,  
775 *Journal of Geophysical Research: Solid Earth*, <https://doi.org/10.1029/2009JB006393>, 114, B10,  
776 2009.  
777
- 778 EMERSITO Working Group. (2024). Rete sismica temporanea 6N installata ad Ancona dal  
779 gruppo EMERSITO durante la sequenza sismica del 2022 - Costa Marchigiana-Pesarese [Data



- 780 set]. Istituto Nazionale di Geofisica e Vulcanologia (INGV).  
781 <https://doi.org/10.13127/SD/QCTGD6C-3A>  
782  
783 Famiani, D., Cara, F., Cultrera, G., Di Giulio, G., et al.: RAPPORTO N. 4 ATTIVITÀ DEL  
784 GRUPPO OPERATIVO EMERSITO A SEGUITO DELL'EVENTO SISMICO Costa  
785 Marchigiana Pesarese Mw 5.5 del 9/11/2022. <http://hdl.handle.net/2122/16014>, in *Italian*, 2023.  
786  
787 Farabollini P., Gentili B., Materazzi M. & Pambianchi G.: Analisi del rischio geo-ambientale: il  
788 bacino del fiume Potenza nelle Marche centrali. Atti X Congr. Naz. Geologi "Il territorio Fragile",  
789 Roma 7-10 dicembre 2000, 575-584, in *Italian*, 2001.  
790  
791 Ferraris, G., Maistrello, M., Rampoldi, R., Secomandi, P., and Stucchi, M.: The seismological  
792 network of Ancona, *Boll. Geof. Teor. Appl.*, 18, 6 8, 299-316, 1975.  
793  
794 Fiorillo, F.: Geological features and landslide mechanisms of an unstable coastal slope  
795 (Petacciato, Italy), *Engineering Geology*, 67, 255–267, 2003.  
796  
797 Guidoboni, E., Ferrari, G., Mariotti, D., Comastri, A., Tarabusi, G., Sgattoni, G., and Valensise,  
798 G.: CFTI5Med, Catalogo dei Forti Terremoti in Italia (461 a.C.-1997) e nell'area Mediterranea  
799 (760 a.C.-1500), Istituto Nazionale di Geofisica e Vulcanologia (INGV),  
800 <https://doi.org/10.6092/ingv.it-cfti5>, 2018.  
801  
802 Hailemikael, S., Amoroso, S., and Gaudiosi, I.: Guest editorial: seismic microzonation of Central  
803 Italy following the 2016–2017 seismic sequence. *Bull Earthquake Eng* 18, 5415–5422,  
804 <https://doi.org/10.1007/s10518-020-00929-6>, 2020.  
805  
806 Istituto Nazionale di Geofisica e Vulcanologia (INGV). Rete Sismica Nazionale (RSN). Istituto  
807 Nazionale di Geofisica e Vulcanologia (INGV). <https://doi.org/10.13127/SD/X0FXnH7QfY>,  
808 2005.  
809  
810 Jurkevics, A.: Polarisation analysis of three-component array data, *Bull. Seismol. Soc. Am.*, 78,  
811 1725–1743, <https://doi.org/10.1785/BSSA0780051725>, 1988.  
812  
813 Kanasevich, E. R.: Time Sequence Analysis in Geophysics, Third Edition, 532 pp., Univ. of  
814 Alberta Press, Edmonton, Canada, 1981.  
815  
816 Kisslinger, C.: The Ancona, Italy Earthquake Swarm, 1972, *Earthquake Notes*, XLIII, 4, 1972.  
817  
818 Konno, K, and Ohmachi, T.: Ground-motion characteristics estimated from spectral ratio between  
819 horizontal and vertical components of microtremor, *Bull Seis Soc Am.*, 88(1):228–241,  
820 <https://doi.org/10.1785/BSSA0880010228>, 1998.  
821  
822 Lettieri M. - Progetto CARG - Il Progetto di Cartografia geologica nazionale alla scala 1:50.000:  
823 stato di avanzamento (novembre 2008), in *Mem. Descr. Carta Geol. d'It. LXXXVIII*, (2009), pp.  
824 17-20 figg. 3  
825  
826 Luzi, L., Lanzano, G., Felicetta, C., D'Amico, M. C., Russo, E., Sgobba, S., Pacor, F., and  
827 ORFEUS Working Group 5: Engineering Strong Motion Database (ESM) (Version 2.0), Istituto  
828 Nazionale di Geofisica e Vulcanologia (INGV), <https://doi.org/10.13127/ESM.2>, 2020.  
829



- 830 McNamara, D. E., and Buland, R. P.: Ambient noise levels in the continental United States,  
831 Bulletin of the Seismological Society of America, 94(4): 1517–1527,  
832 <https://doi.org/10.1785/012003001>, 2004.  
833
- 834 Milana, G., Cultrera, G., Bordoni, P. et al.: Local site effects estimation at Amatrice (Central Italy)  
835 through seismological methods, Bull Earthquake Eng, 18, 5713–5739,  
836 <https://doi.org/10.1007/s10518-019-00587-3>, 2020.  
837
- 838 Moretti, M., Margheriti, L., D’Alema, E. and Piccinini, D.: SISMICO: INGV operational task force  
839 for rapid deployment of seismic network during earthquake emergencies, Front. Earth Sci.,  
840 11:1146579, <https://doi.org/10.3389/feart.2023.1146579>, 2023.  
841
- 842 Nakamura, Y.: A method for dynamic characteristics estimation of subsurface using microtremor  
843 on the ground surface. Railway Technical Research Institute, Quarterly Reports, 30(1), 1989.  
844
- 845 Nardone, L., Vassallo, M., Cultrera, G. Sapia, V. et al.: A geophysical multidisciplinary approach  
846 to investigate the shallow subsoil structures in volcanic environment: The case of Ischia Island,  
847 Journal of Volcanology and Geothermal Research, 438, 107820,  
848 <https://doi.org/10.1016/j.jvolgeores.2023.107820>, 2023.  
849
- 850 PCM-PCD: Presidency of Council of Ministers - Civil Protection Department: Italian Strong  
851 Motion Network [Data set], International Federation of Digital Seismograph Networks,  
852 <https://doi.org/10.7914/SN/IT>, 1972.  
853
- 854 Peterson, J. R.: Observations and Modeling of Seismic Background Noise. U.S.G.S, Open File  
855 Report, 93-322, 95 p., <https://doi.org/10.3133/of93322>, 1993.  
856
- 857 Pischiutta, M., Salvini, F., Fletcher, J. B., Rovelli, A., and Ben-Zion, Y.: Horizontal polarization  
858 of ground motion in the Hayward fault zone at Fremont, California: Dominant fault-high-angle  
859 polarization and fault-induced cracks, Geophys. J. Int., 188(3), 1255–1272,  
860 <https://doi.org/10.1111/j.1365-246x.2011.05319.x>, 2012.  
861
- 862 Pischiutta, M., Cianfarra, P., Salvini, F., Cara, F., and Vannoli, P.: A systematic analysis of  
863 directional site effects at stations of the Italian seismic network to test the role of local topography,  
864 Geophys. J. Int., 214(1), 635–650, <https://doi.org/10.1093/gji/ggy133>, 2018.  
865
- 866 Priolo, E., Pacor, F., Spallarossa, D. et al.: Seismological analyses of the seismic microzonation of  
867 138 municipalities damaged by the 2016–2017 seismic sequence in Central Italy, Bull Earthquake  
868 Eng, 18, 5553–5593, <https://doi.org/10.1007/s10518-019-00652-x>, 2020.  
869
- 870 Reasenber, P. A., and Oppenheimer, D.: FPFIT, FPLOT and FPPAGE: FORTRAN Computer  
871 Programs for Calculating and Displaying Earthquake Fault-Plane Solutions, US Geological  
872 Survey Open-File Report, 85-739, USGS, 109 p., <https://doi.org/10.3133/ofr85739>, 1985.  
873
- 874 Rigano, R., Cara, F., Lombardo, G., and Rovelli, A.: Evidence for ground motion polarization on  
875 fault zones of Mount Etna volcano, J. Geophys. Res., 113, B10306,  
876 <https://doi.org/10.1029/2007JB005574>, 2008.  
877



- 878 Rovida, A., Locati, M., Antonucci, A., and Camassi, R. (a cura di): Archivio Storico  
879 Macrosismico Italiano (ASMI), Istituto Nazionale di Geofisica e Vulcanologia (INGV),  
880 <https://doi.org/10.13127/asmi>, 2017.  
881
- 882 Rovida, A., Locati, M., Camassi, R., Lolli, B., and Gasperini P.: The Italian earthquake catalogue  
883 CPTI15, Bulletin of Earthquake Engineering, 18(7), 2953-2984, <https://doi.org/10.1007/s10518-020-00818-y>, 2020.  
884  
885
- 886 Rovida, A., Locati, M., Camassi, R., Lolli, B., Gasperini, P., and Antonucci A.: Catalogo  
887 Parametrico dei Terremoti Italiani (CPTI15), versione 4.0, Istituto Nazionale di Geofisica e  
888 Vulcanologia (INGV), <https://doi.org/10.13127/CPTI/CPTI15.4>, 2022.  
889
- 890 Spudich, P., Hellweg, M., Lee, W. H. K.: Directional topographic site response at Tarzana  
891 observed in aftershocks of the 1994 Northridge, California, earthquake: Implications for  
892 mainshock motions, Bulletin of the Seismological Society of America, 86, 1B, (S193-S208),  
893 <https://doi.org/10.1785/BSSA08601BS193>, 1996.  
894
- 895 Stucchi, E., Zgur, F., and Baradello, L.: Seismic land-marine acquisition survey on the Great  
896 Ancona Landslide, Near Surface Geophysics, 3.4: 235-243, 2005.  
897
- 898 Stucchi, E., and Mazzotti, A.: 2D seismic exploration of the Ancona landslide (Adriatic Coast,  
899 Italy), GEOPHYSICS, 74, no. 5, 2009.  
900
- 901 Tertulliani, A., Antonucci, A., Berardi, M., Borghi, A., Brunelli, G., Caracciolo, C. H., ... and  
902 Pinzi, S.: Gruppo Operativo Quest Rilievo Macrosismico Mw 5.5 Costa Marchigiana del  
903 9/11/2022, Rapporto Finale del 15/11/2022, <http://hdl.handle.net/2122/15794>, 2022.  
904
- 905 Theodoulidis, N., Cultrera, G., Cornou, C. et al.: Basin effects on ground motion: the case of a  
906 high-resolution experiment in Cephalonia (Greece), Bull Earthquake Eng, 16, 529-560,  
907 <https://doi.org/10.1007/s10518-017-0225-4>, 2018.  
908
- 909 Vassallo, M., Riccio, G., Mercuri, A., Cultrera, G., Di Giulio, G.: HV Noise and Earthquake  
910 Automatic Analysis (HVNEA), Seismological Research Letters, 94 (1): 350-368,  
911 <https://doi.org/10.1785/0220220115>, 2022.  
912
- 913 Wathelet, M., Chatelain, J. L., Cornou, C., Di Giulio, G., Guillier, B., Ohrnberger, M., and  
914 Savvaidis, A.: Geopsy: A User-Friendly Open- Source Tool Set for Ambient Vibration  
915 Processing, Seismol. Res. Lett., 91, 1878-1889, <https://doi.org/10.1785/0220190360>, 2020.  
916  
917

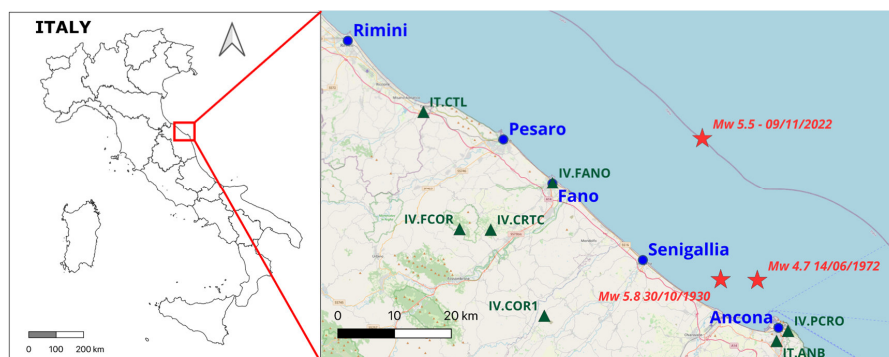




918

## Figures

919



920

921

922

923

924

925

926

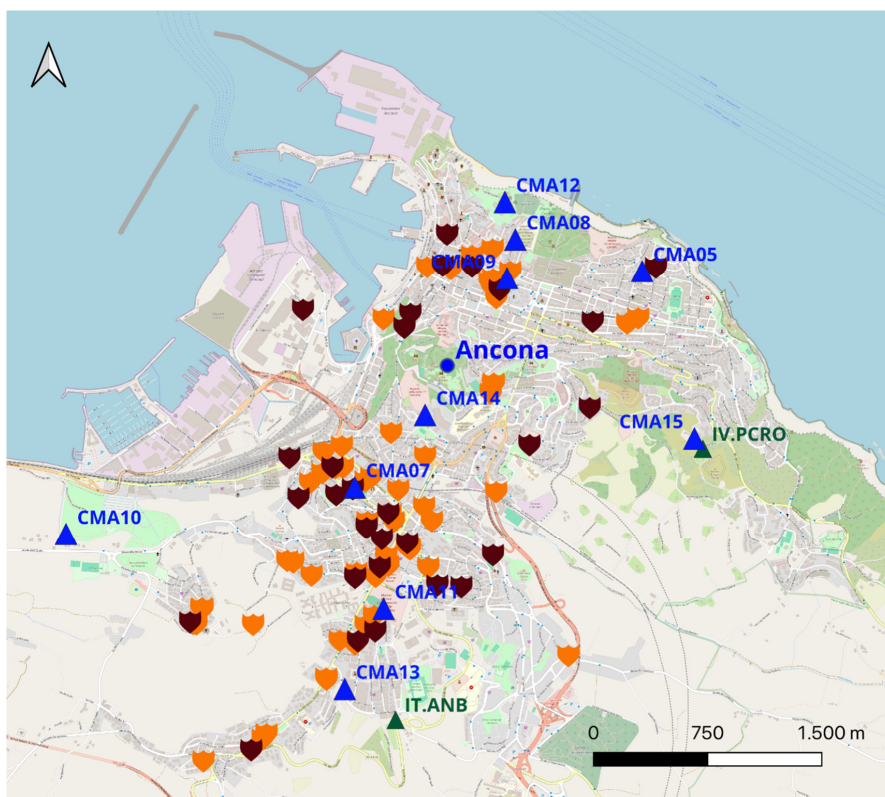
927

**Figure 1.** Left: Map of Italy, the red square indicates the Costa Marchigiana-Pesarese. Right: zoom of the study area showings: a) the epicenter of the MW 5.5 of 09/11/2022 event, and the epicenters of the two strongest earthquakes occurred in the previous century that affected Ancona significantly (red stars); b) the main cities in the Adriatic coast (blue dots); c) the accelerometric stations (green triangles) of RAN and RSN seismic networks closest to the MW 5.5 event.

© OpenStreetMap contributors 2024. Distributed under the Open Data Commons Open Database License (ODbL) v1.0.

928

929



930

931

932

933

934

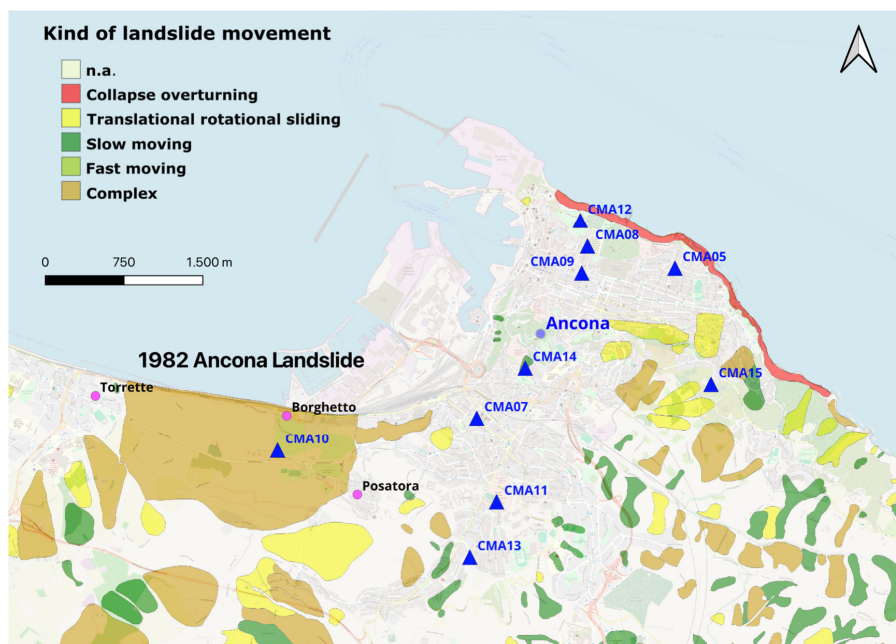
935

936

**Figure 2.** Map of Ancona municipality with the indication of damage reported by the Fire Brigades (from orange to dark-red symbols for increasing intensity, respectively). The blue triangles are most of the stations of the temporary network 6N installed by the EMERSITO working group. The green triangle are the two permanent stations installed at Ancona, IT.ANB and IV.PCRO, respectively.

© OpenStreetMap contributors 2024. Distributed under the Open Data Commons Open Database License (ODbL) v1.0.

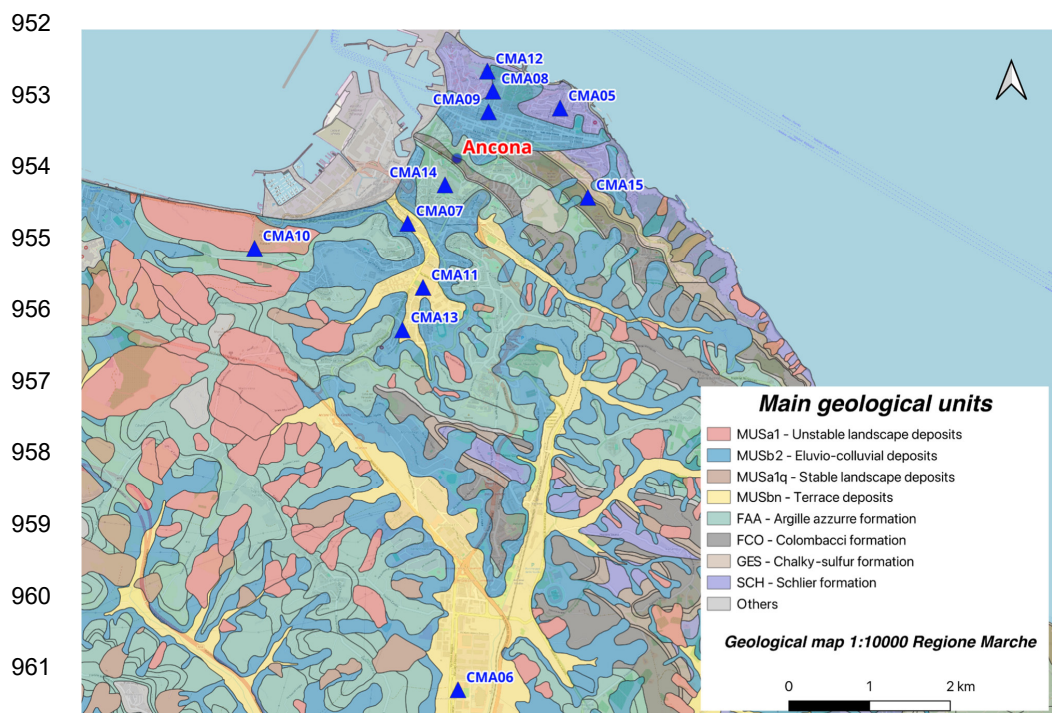
937



938  
939  
940  
941  
942  
943  
944  
945  
946  
947  
948  
949  
950

**Figure 3.** Map of Ancona municipality with landslide phenomena, as carried out by Italian Institute for Environmental Protection and Research (ISPRA) and the Italian Regions and Autonomous Provinces during the project IFFI (Inventory of Landslide Phenomena in Italy). In the map the huge area of the 1982 landslide is highlighted. The magenta dots represent the three districts of Ancona involved in the landslide movement. The blue triangles are most of the stations of the temporary network 6N installed by the EMERSITO working group. The green triangle are the two permanent stations installed at Ancona, IT.ANB and IV.PCRO, respectively. The complete IFFI database is available at the website: <https://www.isprambiente.gov.it/it/progetti/cartella-progetti-in-corso/suolo-e-territorio-1/iffi-inventario-dei-fenomeni-franosi-in-italia>.  
© OpenStreetMap contributors 2024. Distributed under the Open Data Commons Open Database License (ODbL) v1.0.

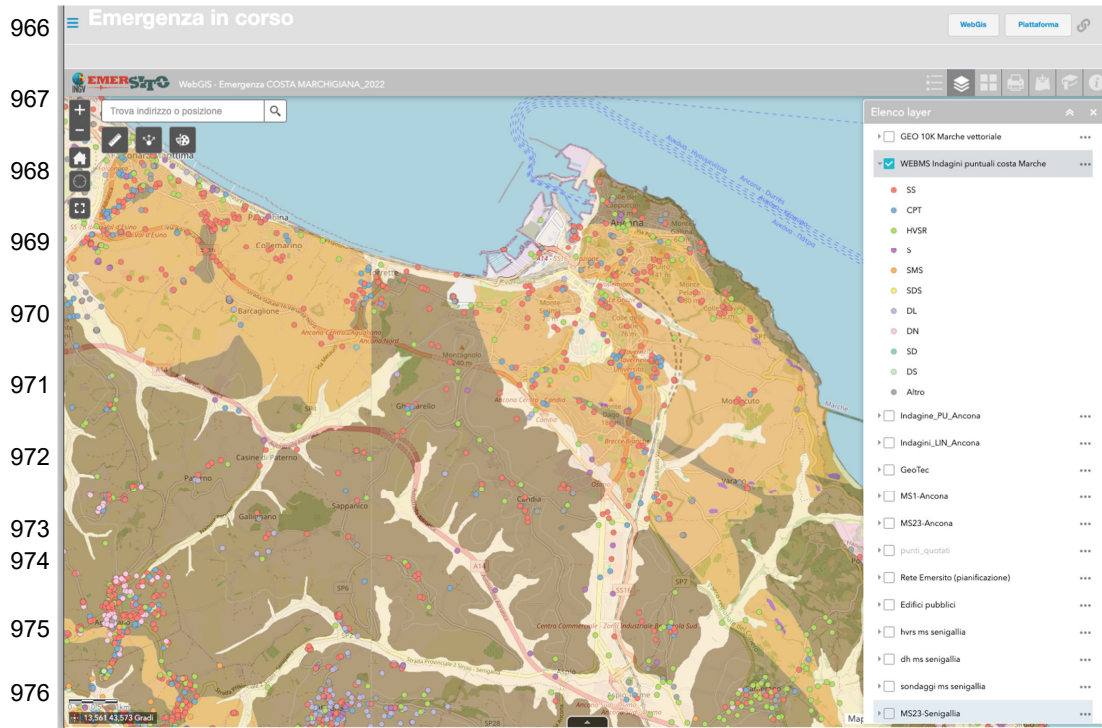
951



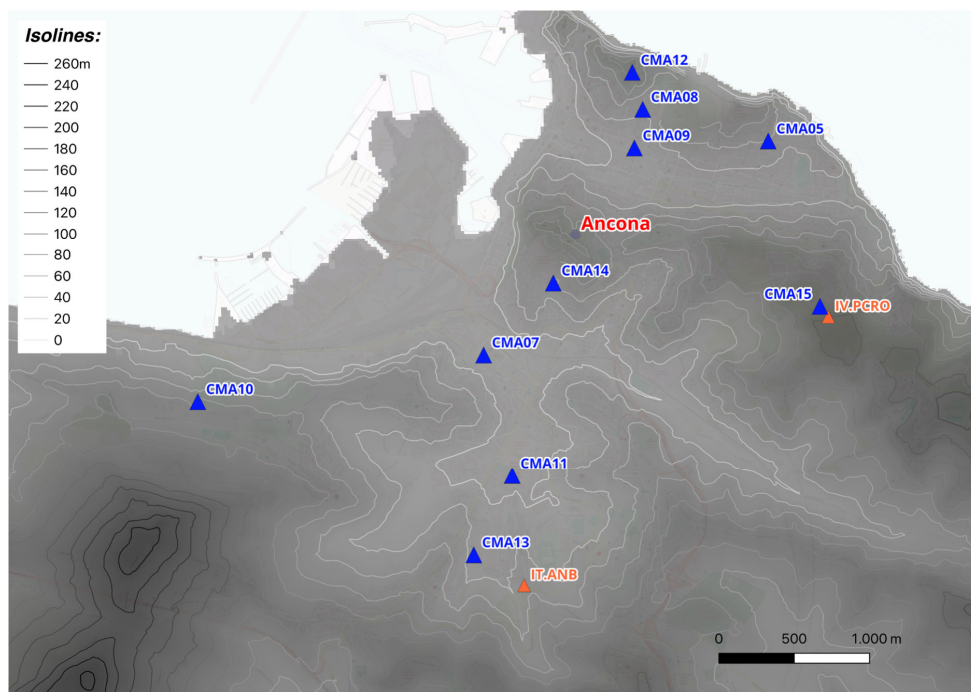
962 **Figure 4.** Geological map (scale 1: 10.000) of Ancona area. Stations of the 6N EMERSITO seismic network (blue triangles)  
963 are superimposed.  
964 © OpenStreetMap contributors 2024. Distributed under the Open Data Commons Open Database License (ODbL) v1.0.



965



977 **Figure 5.** Example of layout used in the online Web-GIS project of EMERSITO, showing the Adriatic coast of Ancona, the  
978 lithological map and the available surveys used in microzonation studies (coloured dots).

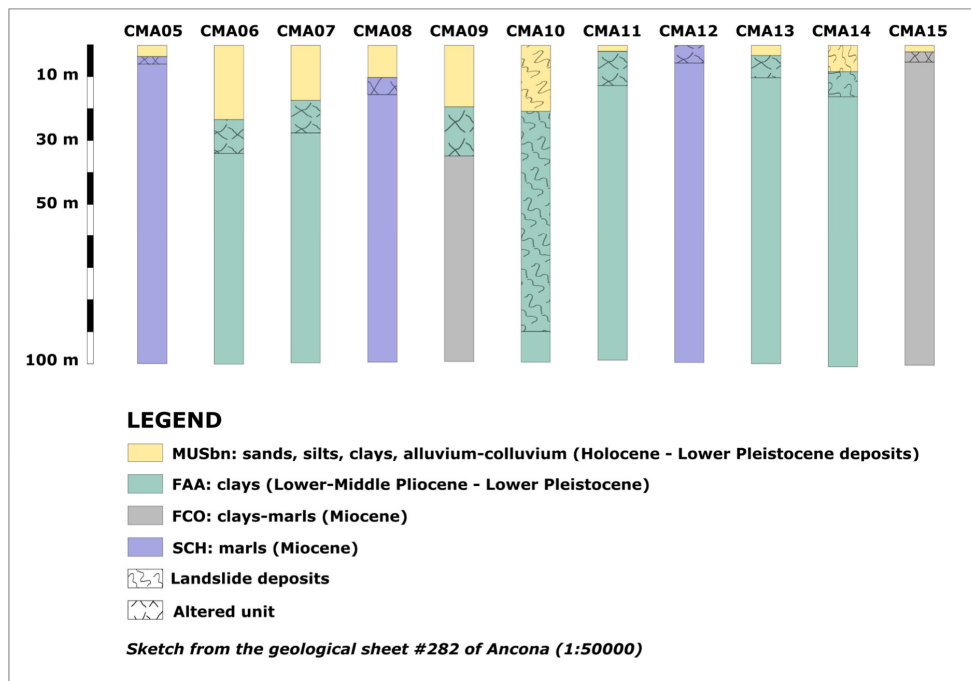


979  
980 **Figure 6.** Topography map with isoline of the Ancona area. The blue triangles are most of the stations of the 6N EMERSITO  
981 Network, the orange triangles are the two permanent stations of RAN (IT.ANB) and RSN (IV.PCRO).  
982 Tarquini S., Isola I., Favalli M., Battistini A. (2007). © TINITALY, a digital elevation model of Italy with a 10 meters cell  
983 size (Version 1.0) [Data set]. Istituto Nazionale di Geofisica e Vulcanologia (INGV). <https://doi.org/10.13127/tinitaly/1.0>

984



985  
986  
987  
988

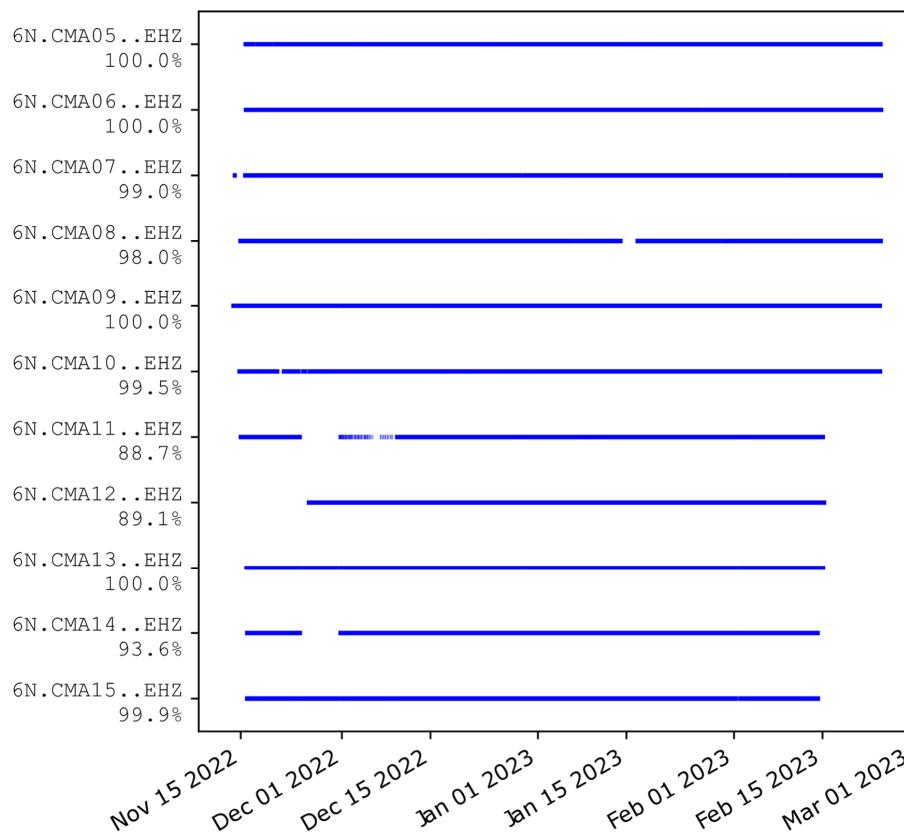


989  
990  
991

Figure 7. 1D stratigraphic models derived at the sites where 6N seismic stations are located.



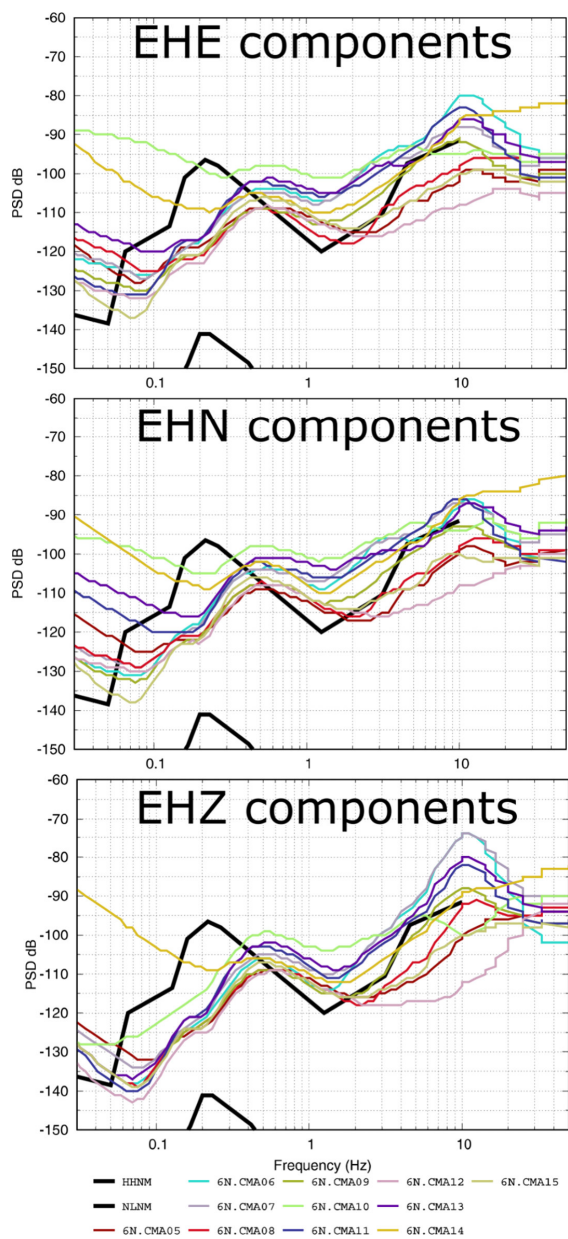
992



993  
994  
995

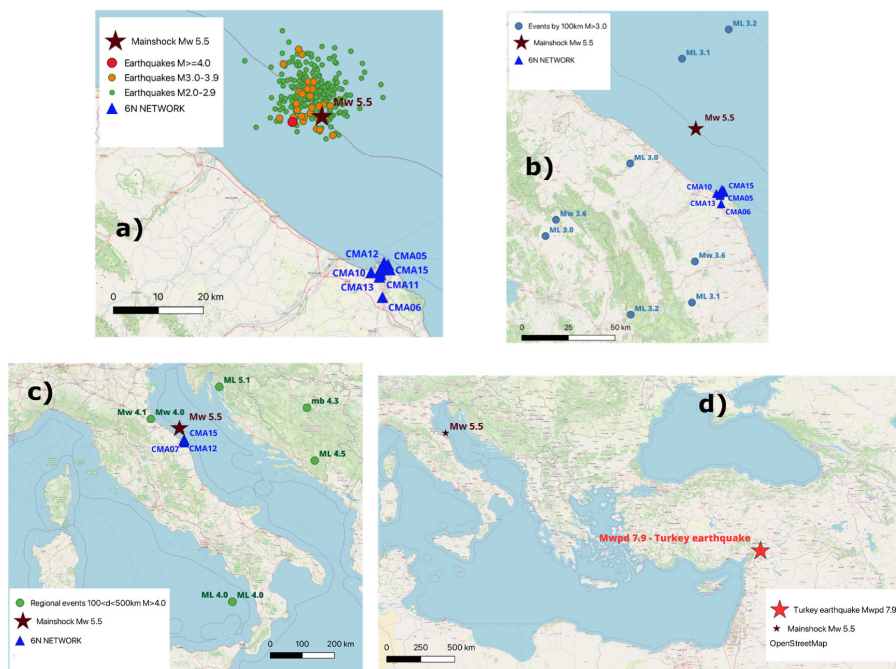
Figure 8. Data availability of the stations of the 6N network during the experiment period.





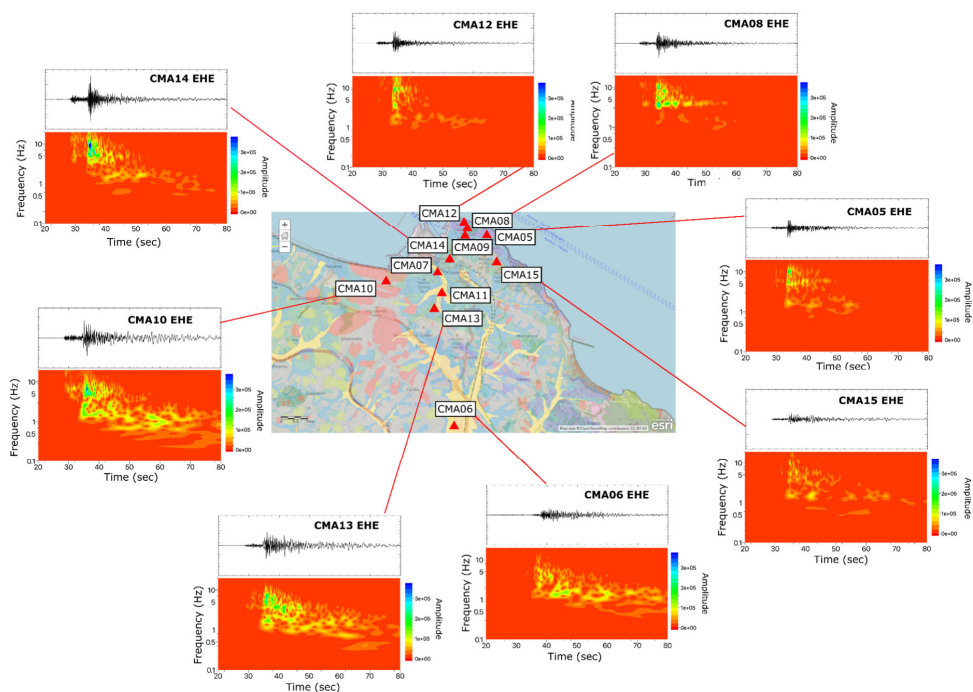
996  
997  
998  
999

Figure 9. 90th percentile curves of PSD computed for all stations on the three components of motion.



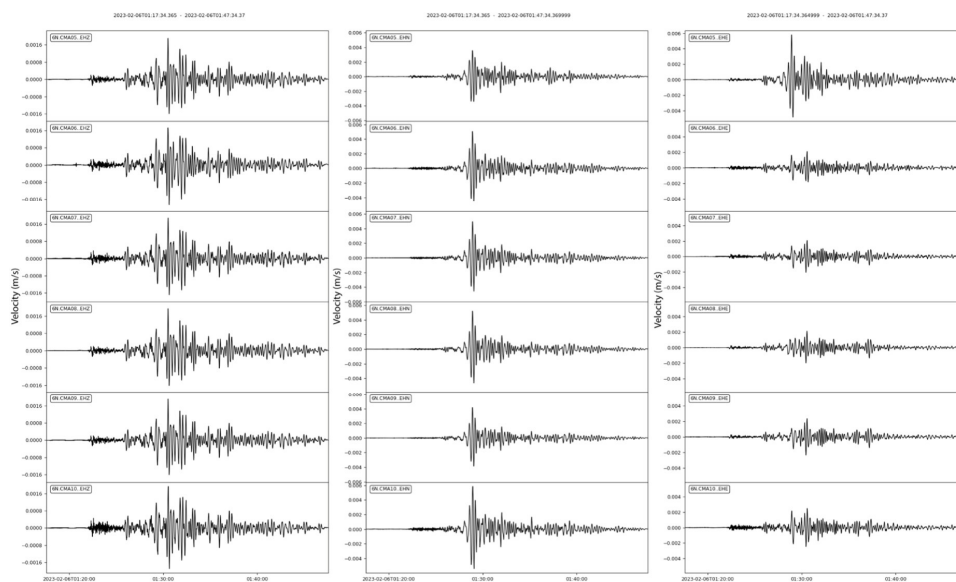
1000  
1001  
1002  
1003  
1004

**Figure 10.** Seismicity during the operation of the 6N network: a) Costa Marchigiana-Pesarese seismic sequence; b) Events of other Italian seismic sources within 100km from Ancona; c) Regional events; d) Telesismic Turkey event.  
© OpenStreetMap contributors 2024. Distributed under the Open Data Commons Open Database License (ODbL) v1.0.



1005  
1006  
1007  
1008  
1009  
1010

**Figure 11.** Time series and spectrograms of the Mw 3.9 earthquake (EHE components) occurred the 8th of December, 2022 at 07:08:18 UTC for some stations of the 6N network.



1011  
1012  
1013  
1014  
1015  
1016  
1017  
1018

**Figure 12.** Seismic traces of the Mw<sub>7.9</sub> Turkish earthquake occurred the 6th of February 2022 (01:17 UTC) recorded by the real-time 6N EMERSITO stations.



1019  
 1020  
 1021  
 1022  
 1023  
 1024  
 1025  
 1026  
 1027  
 1028  
 1029  
 1030  
 1031  
 1032  
 1033  
 1034  
 1035  
 1036  
 1037  
 1038  
 1039  
 1040  
 1041  
 1042  
 1043

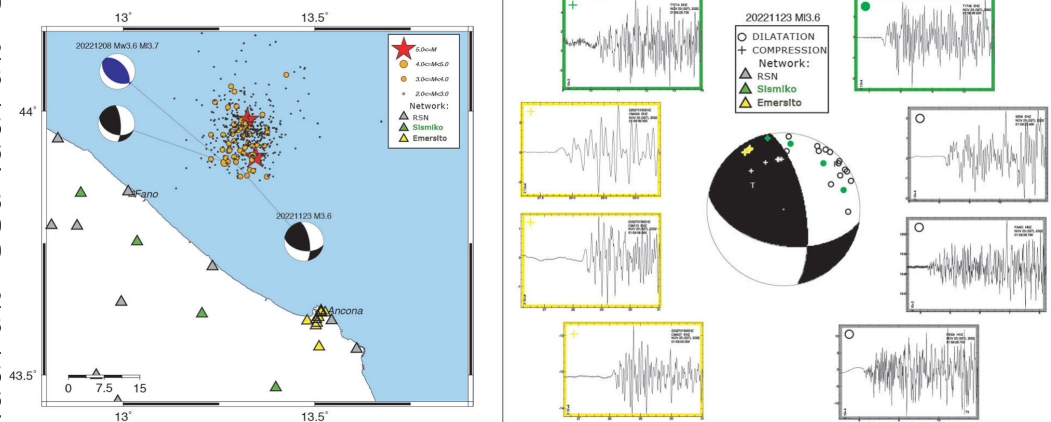
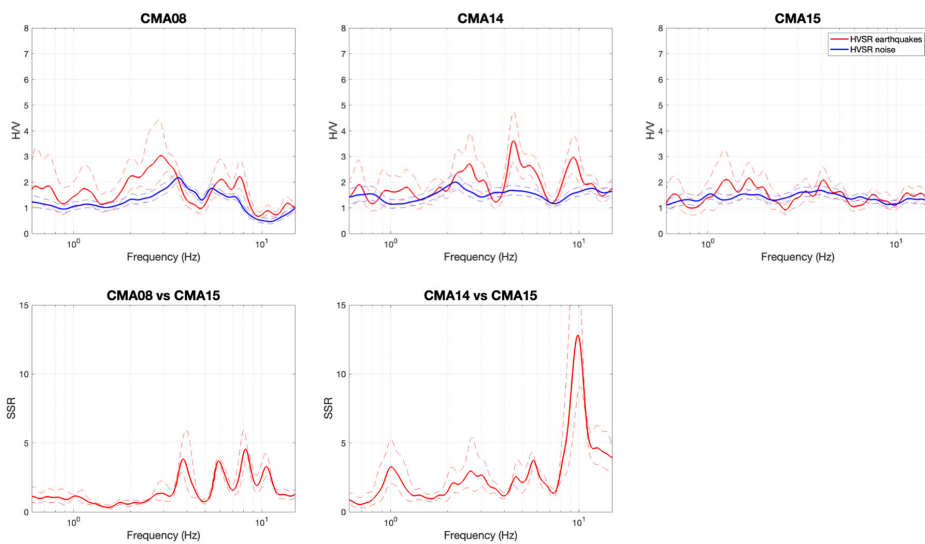
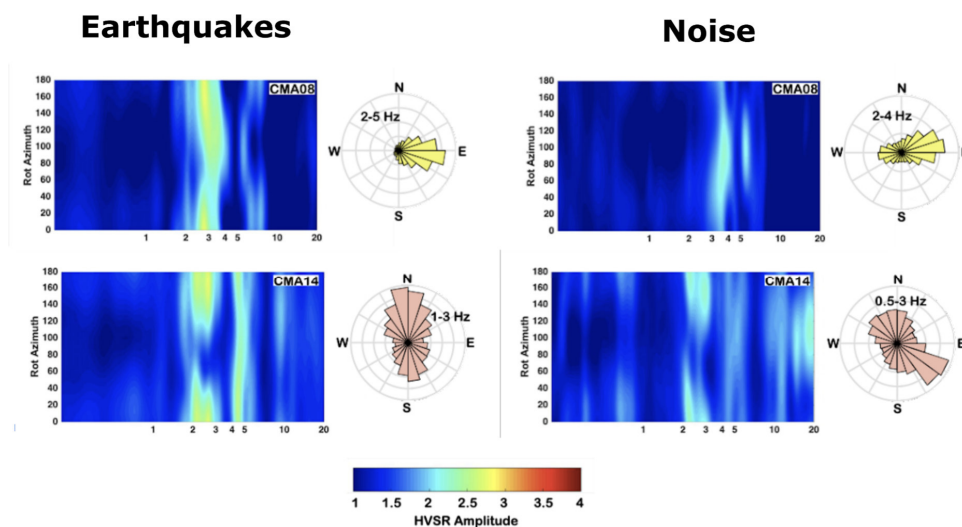


**Figure 13.** Left: Fault-Plane fit (FPFIT) focal solutions (black) for the earthquakes reported in Table 3. For the second event (id #33589291) the available Time Domain Moment Tensor (TDMT) is also shown in (blue); circles are  $M \geq 2.0$  earthquakes of the seismic sequence (see the insert for the different sizes and the correspondence with difference magnitude), and red stars are  $M \geq 5.0$  earthquakes. Right: distribution of polarities, up and down, for the first event in Table 3 (id #33466171). Seismograms recorded by Y1 (green boxes), IV (grey boxes) and 6N (yellow boxes) networks are also shown.



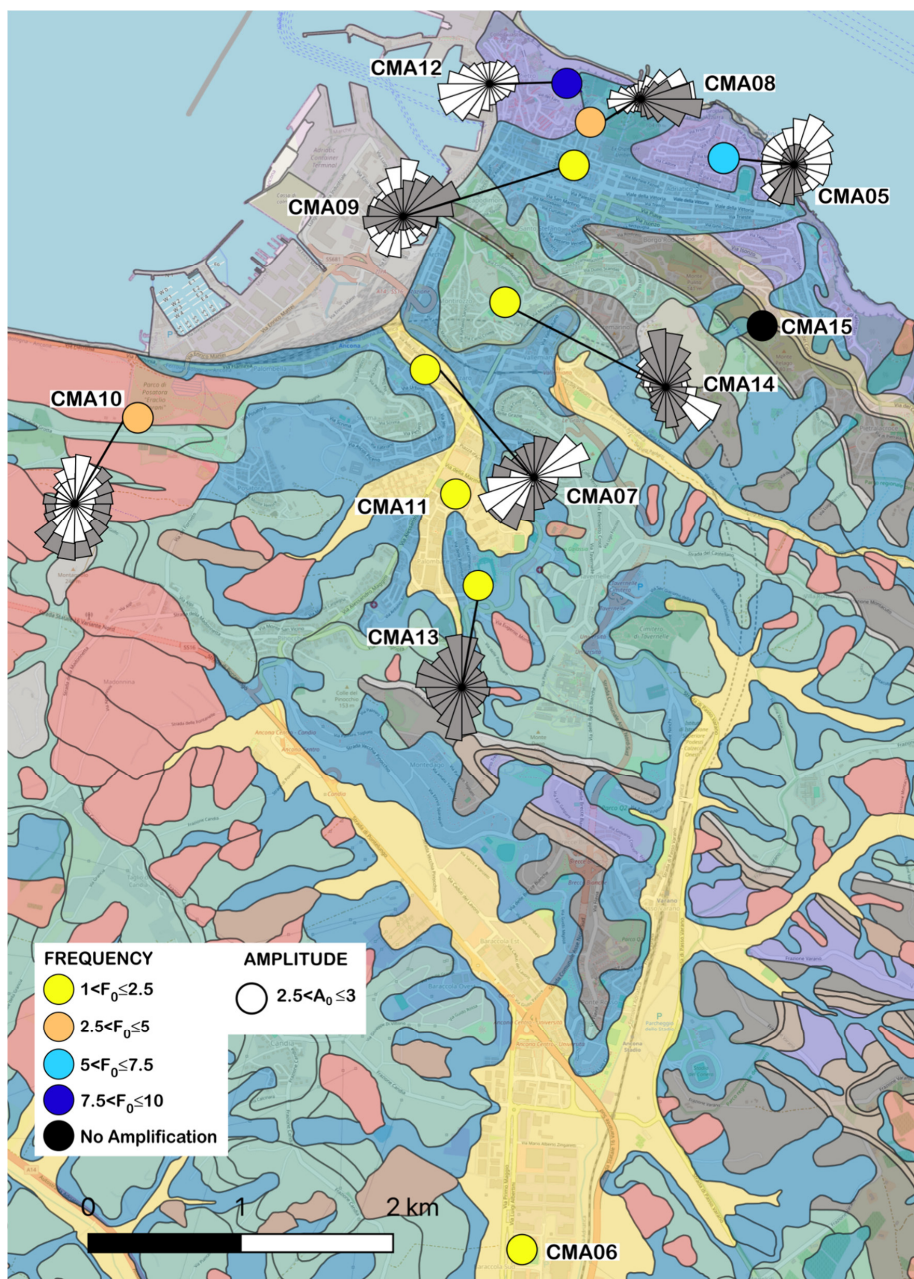
1044  
1045  
1046  
1047  
1048  
1049

**Figure 14.** Top: HVNSR (blue lines) and HVSR (red lines) from HVNEA for CMA08, CMA14 and CMA15 stations. Bottom: SSR for CMA08 and CMA14 stations (red lines). For all plots, the solid lines are the averages, the dotted lines the average minus and plus one standard deviation.



1050  
1051  
1052  
1053  
1054  
1055  
1056  
1057  
1058  
1059  
1060

**Figure 15.** Directional amplification at two exemplificative stations: CMA08 (top) and CMA14 (bottom), by using seismic events (left-hand side) and ambient noise recordings (right-hand side). Rotated HVSR and HVNSR are graphed as contour plots, where the color scale is related to the amplitude level, the x-axis represents frequency, the y-axis the rotation angle ( $0^\circ$  and  $180^\circ$  corresponding to N-S direction,  $90^\circ$  to EW direction). The time-domain polarization analysis is summarized by means of circular histogram diagrams representing the polarization angle in the horizontal plane, obtained from filtered signals in the frequency band indicated in the rose diagram.



1061  
 1062  
 1063  
 1064  
 1065  
 1066  
 1067

**Figure 16.** Summary of the HVSR analyses performed on ambient noise and earthquake recordings, by using only the mean of the two horizontal components and by calculating rotated components. The circle dimension plotted above each station is related to the HVSR  $A_0$  value, while its colour indicates the  $F_0$  value. In case of directional amplification, we also add rose diagrams (gray and white colours are related to results retrieved using earthquakes and ambient noise, respectively). The results are superimposed to the 1:10.000 geological map.  
 © OpenStreetMap contributors 2024. Distributed under the Open Data Commons Open Database License (ODbL) v1.0.